The molecular fingerprint of stress resilience

Bączyńska E.[1], Zaręba-Kozioł M.[1], Ruszczycki B.[1], Krzystyniak A.[1], Wójtowicz T.[1], Bijata K.[1,2], Pochwat B.[1], Magnowska M.[1], Roszkowska M.[1], Figiel I.[1], Masternak J.[1], Dzwonek J.[1], Worch R.[1], Olszyński K.H.[3], Wardak A.D.[3], Szymczak P.[5], Radwańska K.[1], Jahołkowski P.[6], Hogendorf A.[4], Filipkowski R.K.[3], Szewczyk B.[4], Bijata M.[1], Włodarczyk J.[1,*]

[1] Nencki Institute of Experimental Biology, Polish Academy of Sciences; Pasteura 3, 02-093 Warsaw, Poland

[2] University of Warsaw, Faculty of Chemistry; Pasteura 1, 02-093 Warsaw, Poland

[3] Mossakowski Medical Research Institute, Polish Academy of Sciences; Pawinskiego 5, 02-106 Warsaw, Poland

[4] Maj Institute of Pharmacology, Polish Academy of Sciences; Smętna 12, 31-343 Cracow, Poland

[5] Institute of Theoretical Physics, Faculty of Physics, University of Warsaw, Pasteura 5, 02-093, Warsaw, Poland

[6] NORMENT Centre, Division of Mental Health and Addiction, Oslo University Hospital and Institute of Clinical Medicine, University of Oslo, Kirkeveien 166, 0424, Oslo, Norway

*Corresponding author. Email: j.wlodarczyk@nencki.edu.pl

Keywords: *stress-resilient animals, dendritic spines, MMP-9, palmitoylation, chronic unpredictable stress, behavioral stress response*

One Sentence Summary: Compensatory remodeling of dendritic spines at the structural and molecular levels underlies stress resilience.

Abstract: Stress resilience is the ability of neuronal networks to maintain function despite exposure to stress. In this study, we investigated whether stress resilience is an actively developed dynamic process in adult mice. To assess the resilient and anhedonic behavioral phenotypes developed after induction the chronic unpredictable stress, we quantitatively characterized the structural and functional plasticity of excitatory synapses in the hippocampus using a combination of proteomic, electrophysiological, and imaging methods. Our results indicate that stress resilience is a dynamic and multifactorial process manifested by structural, functional, and molecular changes in synapses. We reveal that chronic stress influences palmitoylation, the profiles of which differ between resilient and anhedonic animals. We also observed that stress resilience is associated with structural compensatory plasticity of the postsynaptic parts of synapses.

INTRODUCTION

The resilience phenomenon has been broadly investigated in physics[1–3], geoscience[4], botany[5], ecology[6], sociology[7,8], economics[9], and neuroscience[10,11]. The definition of resilience is not universal and is often determined by researchers based on their own scientific interests[10,12–15]. The common feature of resilience manifests in its dynamic nature, i.e., the ability of a system (e.g., a material, a plant, or a brain) exposed to a harmful stimulus to absorb, accommodate or adapt to the effects of the stress in an efficient manner by adjusting its structure, organization, physiological mechanisms, metabolic regulation, mode of action, etc. The resilience phenomenon is also commonly observed in human neurological diseases, particularly in neurodegenerative and neuropsychiatric diseases[11,16–20]. Despite exposure to traumatic events or even to the presence of advanced pathophysiological changes, some people do not exhibit behavioral and psychological symptoms. The origin of such a diverse response to stressful conditions at the level of brain plasticity is an unexplored field of modern neuropsychiatry and neuroscience. The functional capacity resulting from individual predispositions that determine the degree of the organism's adaptation to changes in the state of health is the basis of the stress-resilient phenotype[21–24]. Many researchers point to the principal role of genetic predispositions in stress resilience, while others see its origin in protective factors, reward system, brain reserve or aberrant functions of key molecules[22,25–30]. Despite the broad research in this field, the impact of the environmental factors contributing to stress resilience is still largely unexplored. One of the fundamental questions that still lacks a clear answer is whether the stress resilience developed during adulthood might be an actively regulated process[31]. Several findings indicate that stress resilience can be pharmacologically enhanced upon treatment with glutamate receptor antagonists, e.g., ketamine[29,32–35]. However, the changes in the molecular landscape underlying drug-induced stress resilience have not yet been identified in the treatment of stress-related disorders.

Major depressive disorder (MDD) is one of the commonly occurring forms of stress-related disorders and has been extensively studied both in humans and in animal models[36,37]. The etiology of MDD is complex and idiopathic. Many factors influence the development of MDD, including genetic predispositions and the environment[38,39]. Nevertheless, chronic stress is a key contributor to MDD development due to its impact on the dysregulation of the hypothalamic–pituitary–adrenal axis and adrenal steroids[40,41]. Observations of the diverse distribution of glucocorticoid receptors within brain regions reveals the medial prefrontal cortex, hippocampus, and amygdala as the

structures most affected by chronic stress in MDD patients and animals displaying depressive-like behavior[41–43]. Of importance, the broad, interdisciplinary characterization of the hippocampus enables the integration of molecular, functional, and imaging data in the context of animal behavior. Moreover, *postmortem* studies of MDD subjects revealed that antidepressive action requires synaptic plasticity in the hippocampus[44,45]. Multiple studies postulate that the mechanisms of MDD are described by the theories of the monoamine-, inflammation-, neurotrophy-, circadian- or GABA-glutamate mediated hypotheses[46,47]. However, none of them is convincing enough to explain the molecular mechanism or the combination of all of the symptoms and subtypes of MDD[46,47]. Nevertheless, all these theories share a common concept that aberrant synaptic plasticity underlies depressive symptoms and that pathology-related structural changes are caused by the increased excitatory transmission induced by chronic stress[41,48–51]. Furthermore, the restoration of excitatory structural connectivity in the rodent hippocampus and prefrontal cortex with ketamine, a fast-acting NMDA antagonist, is sufficient to return animals to a healthy behavioral state[52–55].

The changes in structural connectivity are related to the processes occurring in the excitatory synapses[56]. Most of the excitatory synapses are located on dendritic spines, which are small, motile membrane protrusions of neurons[57]. Dendritic spine remodeling involves alterations in spine morphology and/or density[56]. The structural plasticity of dendritic spines is a hallmark of physiological (learning and memory) and pathological (neurological and neuropsychiatric disorders) conditions[58–60]. Studies of depressive-like behavior in animal models revealed abnormalities in the maintenance of the strength of synaptic connections that were manifested by a loss of spines and/or an increase in the proportion of immature, thin forms of spines. This finding suggests that the mechanism responsible for the transformation of dendritic spines might be a key factor underlying depressive-like behaviors[60,61]. However, this phenomenon appears to be more complex due to the observations that dendritic spine remodeling is not necessary for the short-term antidepressant effect of ketamine, but it may be essential to sustain the remission of depressive-like behavior[54,55,62]. These studies point out the downstream signaling pathways underlying the regulation of dendritic spine shape and function as a possible decisive molecular target for promoting stress resilience and preventing pathogenesis.

Dendritic spine structure is regulated by the reorganization of the actin cytoskeleton, scaffolding proteins, and extracellular matrix proteases, e.g., matrix metalloproteinase 9 (MMP-9) and small

Rho GTPases, e.g., CDC42[63–66]. MMP-9 is secreted extracellularly upon neuronal stimulation, therein activating the NMDA receptor[63,64,67–69]. Many studies indicate aberrant structural plasticity of dendritic spines and elevated activity of MMP-9 as hallmarks of the depressive state[70–74]. However, there are no reports describing how the structure of dendritic spines and the underlying molecular landscape of the tetrapartite synapse are affected in resilient animals following chronic stress and how components of the tetrapartite synapse regulate this process. Recently, S-palmitoylation (S-PALM) has gained attention due to its role in stress-related neuropsychiatric diseases[75] and the remodeling of dendritic spines[76,77]. S-PALM is a fast-acting posttranslational lipid modification in which palmitic acid is attached to cysteine residues in peptides and proteins. S-PALM is one of the most unique posttranslational modifications because, unlike other lipid modifications, S-PALM is reversible[78,79] and may be regulated by the neuronal activity triggered by environmental factors[80] or pharmacological treatment[77]. S-PALM controls protein stability, receptor trafficking, and protein–protein interactions and thus contributes to synaptic plasticity, e.g., modulation of long-term potentiation (LTP)[76,80–82]. However, the role of S-PALM in stress resilience and the contribution of S-PALM to the dendritic spine remodeling is still an open subject and requires further study.

In the present study, we address the following questions: *i)* Is stress resilience a dynamic process that is actively developed in the adult brain?; *ii)* To what extent does chronic stress affect the molecular architecture of the synapse in resilient and anhedonic animals?; *iii)* Are the differences between resilient and anhedonic animals related to the structural and/or functional plasticity of excitatory synapses?; *iv)* Is it possible to explain the potential differences in underlying synaptic plasticity between resilient and anhedonic animals in terms of the palmitoylation of synaptic proteins?; *v)* Is MMP-9 activity in the hippocampus a biomarker of depressive/resilient state?

To answer the aforementioned questions, we applied chronic unpredictable stress (CUS) leading to the development of resilient and anhedonic behavior, establishing a novel animal model of stress resilience. The evaluation of the functional, structural, and molecular readouts of excitatory synaptic plasticity in the hippocampus, in relation to animal behavior, was performed by a multidisciplinary and quantitative methodological approach that include mass spectrometry, electrophysiology, and fluorescent confocal imaging. The presented results indicate that stress resilience is a multifactorial phenomenon that actively develops during adulthood. Moreover, we

demonstrate that the developed stress-resilient state is associated with aberrant synaptic plasticity at the structural, functional and molecular levels.

RESULTS

Chronic stress leads to the development of stress resilience and anhedonia in adult mice

To investigate whether stress resilience might develop during adulthood, we employed CUS to induce a behavioral stress response in adult animals. Ten-week-old male C57BL6J mice were subjected to 2-weeks of chronic and unpredictable stress in which different types of stressors (restraint stress, social defeat stress, tail suspension stress, predator-induced stress) applied in a pseudorandom manner on consecutive days within the dark and light phases of the 12/12 cycle (see *Materials and Methods* for details). We demonstrated that the implementation of such an intense CUS procedure leads to the development of anhedonic and resilient behaviors, as determined by the sucrose preference test (SPT, Figure 1A-C). Anhedonic mice were considered by sucrose preference following chronic stress (SPT1) < 70.7% (defined by the difference between the control and stressed groups being higher than the two standard deviations (>2xSD) established in our recent studies[74]). In turn, mice were considered stress resilient after CUS when they did not exhibit anhedonia in SPT1 (sucrose preference > 70.7%). After CUS, 50% ± 9% of mice developed anhedonic behavior, and the rest were classified as stress-resilient (Figure 1C). Moreover, mice subjected to CUS (both anhedonic and resilient) exhibited less robust body weight gain than that of the nonstressed control animals. Thus, body weight constitutes a physiological indicator of exposure to chronic stress (Figure 1D)[83,84]. Furthermore, we investigated whether the animals following CUS are sensitive to antidepressive treatment. The experimental design and results are outlined in *Supplementary Materials Figure 1A-B*. We observed that the antidepressive effect of ketamine seems to be reached in the anhedonic group, while resilient animals did not respond for ketamine treatment (*Supplementary Materials Figure 1C*). Taken together, our data indicate that implementation of the designed CUS procedure leads to the synchronic development of anhedonic and resilient behavior in genetically homogenous adult mice, constituting a promising animal model of stress resilience. Finally, for further analysis of synaptic plasticity in the hippocampus, we chose representative animals within behavioral groups whose behavioral parameters (SPT1, FST, weight) are outlined in Figure 1E-G.

Chronic stress affects the expression of synaptic proteins in the hippocampus

As a first step to determine the molecular fingerprint of stress resilience, we employed a high-throughput proteomic approach using mass spectrometry to generate a comprehensive view of the *in vivo* protein level in the hippocampal synaptoneurosomes of control, resilient and anhedonic animals. To isolate synaptoneurosomes we used a previously established method that relies on ultracentrifugation and a density gradient[85,86]. We evaluated the quality of the synaptoneurosome preparation using electron microscopy (see *Supplementary Materials Figure 2).* To identify differentially expressed proteins across behavioral groups, their protein levels were determined and comparatively analyzed in five biological replicates per group. Additionally, the clustering heatmaps of Pearson correlation coefficients (PCCs) of peptide signal intensity were determined using logarithm 2 transformed protein abundance data (Figure 2A) to evaluate the variability in the proteomic analysis within biological replicates and behavioral groups. The correlation matrix shows the PCC values for all experimental groups. The matrix values for each stressed group differed from the matrix values for the control group. Moreover, the variation in the matrix values for the control group was small, in contrast to the variations for the other two groups (Figure 2A). Volcano plots depict the changes in protein expression among behavioral groups (Figure 2B). The fold change logarithm (base 2) is on the x-axis, and the negative logarithm of the false discovery rate (p value) (base 10) is on the y-axis. Protein levels with p value <0.01 and fold changes <-1 and >1 were considered significantly different. We identified 6224 proteins with less than 1% FDR (false discovery rate). Our results revealed 44 differential synaptic proteins in resilient animals (24 upregulated and 20 downregulated) and 39 in the anhedonic group (20 upregulated and 19 downregulated) in comparison to nonstressed animals. The list of the proteins within the aforementioned groups is presented in *Supplemental Tables 1A-B.* Surprisingly, the levels of only 6 synaptic proteins significantly differed between the resilient and anhedonic groups: Ppp3ca, Recql, Tenm1, Fastkd1, Gcc2 and Zdhhc13 (one downregulated and five upregulated; for more details, see *Supplemental Table 1C*). Altogether, chronic stress regulated less than 1% of the identified synaptic proteins in the hippocampus.

Chronic stress impairs postsynaptic glutamatergic neurotransmission in the hippocampus

Since we did not observe global changes in protein levels in the hippocampus after chronic stress, we studied synaptic transmission by recording field excitatory postsynaptic potentials (fEPSPs) in acute hippocampal brain slices. To determine the α-amino-3-hydroxy-5-methyl-4-

isoxazolepropionic acid receptors (AMPARs) and *N*-methyl-D-aspartate receptors (NMDARs) that contributed to synaptic transmission, we analyzed fEPSPs evoked in response to monotonically increased stimuli in CA3-CA1 hippocampal projections in magnesium-free aCSF[87]. Input–output curves showed that the amplitudes of the AMPAR-mediated fEPSPs were significantly lower in both the anhedonic and resilient groups as than in the controls ($p < 0.0001$ and $p < 0.0001$, respectively, one-way repeated-measures ANOVA, with Dunnett's post-hoc test, data not shown). Similarly, the area of the NMDAR-mediated component of fEPSPs was significantly lower in both the anhedonic and resilient groups than in the controls ($p < 0.0001$ and $p > 0.0002$, respectively, one-way repeated-measures ANOVA, with Dunnett's post-hoc test, data not shown). Surprisingly, we observed the largest difference in the amplitudes of the fiber volley, which was significantly higher in the anhedonic group but significantly lower in the resilient group than in the controls ($p < 0.0001$, both, one-way repeated-measures ANOVA, with Dunnett's post-hoc test, Figure 3A). The observed differences reflect changes in presynaptic axon function and/or the number of available afferent fibers following chronic stress[88]. Therefore, we visualized the fEPSP amplitude and the area vs. respective fiber volley amplitudes preceding these synaptic responses (Figure 3B-C). We found that the magnitude of AMPAR-mediated fEPSPs recorded for the same fiber volley amplitude was less pronounced in anhedonic but not in resilient animals than in controls (Figure 3B). In contrast, NMDAR-mediated fEPSPs did not differ among the experimental groups of animals (Figure 3C).

Subsequently, we performed three-dimensional Monte Carlo simulations that incorporated fiber volley, fEPSP, and stimulus intensity (see *Materials and Methods* for details) to quantify the efficacy of synaptic transmission in response to stimulation of a similar number of presynaptic afferents. Monte Carlo simulations showed that the amplitude of AMPAR-mediated fEPSPs but not of NMDAR-mediated fEPSPs normalized to the fiber volley amplitude was significantly lower in the anhedonic group than in the control and resilient groups (Figure 3B-C). Therefore, stimulation of the same number of presynaptic afferents yielded less efficient excitatory AMPAR-mediated synaptic drive in the anhedonic group.

Consequently, we investigated whether chronic stress is associated with an altered AMPAR/NMDAR ratio. To this end, we compared the sensitivity of compound fEPSPs to an AMPAR-specific antagonist (DNQX), as described previously[89]. We found a lower

AMPAR/NMDAR ratio in the resilient group than in the anhedonic group (Figure 3D). The potentiation of synaptic release in response to paired-pulse stimulation was similar among the investigated groups (Figure 3E). Therefore, an altered presynaptic release was not attributed to any behavioral phenotype. Taken together, chronic stress affects glutamatergic neurotransmission in the hippocampus differently in the anhedonic group (less efficient excitatory drive and an increased AMPAR/NMDAR ratio) than in the resilient group. Since the observed functional alterations in the CA1 region of the hippocampus were limited to the postsynaptic part of the excitatory synapses, we subsequently analyzed the structural features of dendritic spines.

Stress resilience is associated with structural compensation in the hippocampus

To determine how chronic stress affects dendritic spine structure, we performed DiI staining on hippocampal slices obtained from the second hemisphere and visualized them by fluorescence confocal microscopy. In the analysis of the hippocampus, we observed that the resilient animals differed from the control animals with respect to dendritic spine morphology. The spine density of the resilient animals was unchanged, while in the anhedonic group, decreased spine density was observed ($p < 0.0001$, Figure 4A-C). The quantitative analysis of spine morphometry showed a decreased *length-to-head-width* ratio and spine *area* in the resilient group than in the controls ($p < 0.05$), indicating spine maturation (Figure 4B-C). In summary, we conclude that resilient behavior is accompanied by structural compensation in the hippocampus, which is shown in the representative confocal images of dendritic spines in Figure 4D.

Distinctive palmitoylation of structural synaptic proteins in stress resilience

We hypothesized that the structural compensation of dendritic spines observed in resilient animals might be explained by the dynamic process of altered synaptic protein expression or protein posttranslational modifications. In this regard, S-palmitoylation (S-PALM) could potentially be involved due to its known role in brain pathology[75] and in the structural plasticity of dendritic spines[77]. We therefore took an unbiased proteomic approach based on the mass spectrometry PANIMoni method (the biotin labeling of S-palmitoylated proteins)[85] to identify proteins palmitoylated in response to the CUS procedure. We examined the level of similarity of protein content within the groups using principal component analysis (PCA) and clustering heatmaps of Pearson correlation coefficients (PCCs). We confirmed the reproducibility of the proteome preparation, enabling us to observe a global distinction between the control and stressed mice in

the S-PALM profile of synaptic proteins. The results of the relative quantification experiment are summarized in Figure 5A-D. We identified S-PALM of 1199 synaptic proteins upon the CUS procedure in which 113 proteins were commonly changed in the same direction with a fold change of > 1.25 and q < 0.05 for all stressed mice, while 188 of synaptic protein differentiated the resilient phenotype from those of the anhedonic and control animals, constituting the S-PALM fingerprint of stress resilience (*Supplemental Table 2A*). To determine which cellular and synaptic processes were involved in stress resilience-induced turnover of palmitoylation, we analyzed the datasets of differentially palmitoylated proteins using the synaptic protein database ClueGO. In the ClueGO analysis, we identified functionally grouped networks linked to their GO biological processes and KEGG pathways, indicating palmitoylation-dependent biological processes that were associated mostly with the glutamate receptor signaling pathway (e.g., Daglb, Frrs1, Grin2b, Plcb1, Ptk2b, Shank3, Crtc1, Epha4, Rab3a,Tbc1d24), dendritic spine morphogenesis (e.g., Epha4, Kif1a, Shank3, Tanc2, Ptk2b, Tbc1d24, Erc1, Rab3a), receptor clustering (e.g. Grin2b, Lrp4, Shank3), synaptic vesicle turnover and localization (e.g., Ap3d1, Ap3m2, Htt, Kif1a, Rab3a, Shroom2, Tanc2, Ykt6, Tbc1d24, Ppp3cb), dopamine secretion (e.g., Abat, Kcna2, Prkcb, Rab3a, Syt3), and behavioral fear response (e.g., Grin2b, Shank3, Vdac1), (Figure 5E-F).

MMP-9-dependent behavioral stress response

Having identified specific changes at the synapse and in dendritic spine structure, we hypothesized that MMP-9 activity might trigger the differentiation of S-PALM within behavioral groups. We recently demonstrated that the activation of MMP-9/CDC42 signaling pathway leads to the development of depressive-like behavior and dendritic spine remodeling in the hippocampus[74]. To determine the MMP-9 and CDC42 activities in the hippocampus, we used gel zymography as well as CDC42 pull-down analysis combined with Western blotting, as described previously[74]. We observed activation of the MMP-9/CDC42 signaling pathway in anhedonic animals, while the activities of MMP-9 and CDC42 in the hippocampus were not different between resilient animals, and the controls (Figure 6A-G). Taken together, these results indicate that MMP-9 activity may be a decisive regulator of synaptic plasticity as well as the behavioral stress response upon chronic stress.

DISCUSSION

In the present study, we aimed to investigate whether stress resilience is an actively-developed dynamic process in adult mice. Therefore, we determined the molecular fingerprint of stress-resilient behavior involved in hippocampal neuronal circuits upon chronic stress. We demonstrated that stress resilience is associated with alterations in glutamate receptor signaling pathways, which are exclusively limited to the postsynaptic parts of synapses. We showed that stress resilience manifests itself by compensatory remodeling of dendritic spines, combined with concomitant changes in the S-PALM of synaptic proteins involved in spine morphogenesis, receptor trafficking and glutamatergic neurotransmission.

The complex characterization of synaptic plasticity in resilient animals is an appealing issue. Most of the research on stress resilience is related to a behavioral evaluation in early-life maternal separation models or to the genetic knockouts of targeted proteins that promote stress-resilient behavior in adulthood[21,90,91]. Therefore, we discuss our results with respect to those animal models that share similar components of stress procedures to those of models based on the chronic unpredictable stress and social defeat paradigms. Moreover, because dendritic spine remodeling is modulated mainly by receptor membrane trafficking, MMP-9 activity, mTOR-dependent signaling pathways[64,92,93] and because ketamine evokes antidepressive effects, we decided to emphasize the mechanisms of MMP-9 activity and ketamine action as the main references for further considerations. According to the literature, MMP-9 activity is one of the principal regulators of dendritic spine structure in the hippocampus and is a key marker of synaptic plasticity[63,64,67–69]. In particular, MMP-9 has recently attracted attention due to its contribution to the development of depressive states. Elevated MMP-9 levels in the serum of MDD patients and activity in the hippocampus of anhedonic animals following CUS have been described[70–72,74]; however, the role of MMP-9 activity in stress resilience is still unexplored.

As a result of the multifaceted and comprehensive analysis of the characteristics of the resilient and anhedonic phenotypes, which differ from those of the nonstressed mice, we observed specific changes in synaptic plasticity within behavioral groups. Similar to reports in the literature[94–97], we observed significant differences in the expression levels of synaptic proteins following chronic stress, but those changes did not differentiate the resilient and anhedonic phenotypes. Importantly, the ClueGO analysis revealed that significantly altered expression levels of the synaptic proteins

associated with chronic stress was particularly associated with morphogenesis of dendritic spines and processes related to protein localization to the postsynaptic membrane, which is in agreement with the results of the aforementioned studies.

Several authors noticed robust proteomic alterations in the hippocampus following chronic stress[94,98,99]. However, our results revealed more subtle changes than those of the results reported earlier. This difference may be because we used the synaptoneurosomal fractions and not brain homogenates from the entire hippocampus.

Chronic stress has been shown to affect glutamatergic neurotransmission in the hippocampus as well as learning and memory[100–102]. In our study, we focused on the general characteristics of the AMPAR- and NMDAR-mediated fEPSPs in each behavioral group. We did not aim to assess how the chronic stress affects LTP and learning and memory in mice. Nevertheless, our CUS protocol was based on that in a study by Strekalova et al. (2004, 2010)[103,104] in which behavioral evaluation for learning and memory was performed, showing cognitive impairments in anhedonic animals. This experimental direction is particularly worth investigating in the future, as studies in humans have shown that resilient individuals exhibit cognitive enhancement[105,106].

The potential cognitive enhancement in the resilient animals may arise from the structural compensation of dendritic spines in the hippocampus (manifested by the higher spine density and levels of the observed spine maturation of already existing spines than those in the anhedonic group). The importance of appropriate restoration of the density and morphology of dendritic spines is emphasized in strategies of MDD treatment[58,60,62,107]. In particular, the results obtained in preclinical studies concerning the activity of fast and long-acting antidepressants, such as glutamate-based antidepressants, e.g., ketamine, or serotonin-based compounds, such as psilocybin, have shown that sustained antidepressant-like effects could causally depend on changes in the density and/or morphology of dendritic spines[93,108,109]. In general, not every type of stress protocol similarly affects the structure of dendritic spines. In fact, only severe and prolonged exposure leads to pathological remodeling of spines (density and/or morphology), which is assumed to be a structural correlate of depressive symptoms in rodents[110]. In the present study, we showed that anhedonic animals exhibited a decrease in spine density with morphometric changes within the whole hippocampus. However, we have recently demonstrated[74] that anhedonic behavior also correlates with spine elongation in the CA1 subregion of the hippocampus and that

this subregion of the hippocampus is exclusively involved in the development of anhedonic behavior[74]. Therefore, the lack of changes in the morphology of dendritic spines observed here in the anhedonic group in comparison to control group may be due to the fact that all hippocampal regions (CA1, CA3, DG) were combined into a single analysis assessed to compare the structural alterations of spines with mass spectrometry analysis performed on the synaptoneurosomal fraction obtained from the entire hippocampus. Further research in the hippocampal subregions and other brain structures would be beneficial to better understand the potential mechanism of structural compensation occurring in resilient animals.

In line with the results of other studies[111–113], we did not observe differences in the expression levels of synaptic proteins belonging to the mTORC1 complex following chronic stress. Nevertheless, the reduced level of Rictor protein (mTORC2 binding partner) in the resilient group gained our attention due to mTORC2 insensitivity to the rapamycin[114]. The role of mTORC2 in the hippocampal synaptic plasticity has been widely reported[115–117]. However, how its complex may be engaged in the behavioral stress response and how it is palmitoylated have not yet been studied. Nevertheless, we also observed differences in the palmitoylation (Cys-162) of tetratricopeptide repeat ankyrin repeat and coiled-coil containing 2 (TANC2) between the resilient and anhedonic animals and the controls. Deletion of TANC2 in the hippocampus hyperactivates mTORC1/mTORC2-dependent signaling pathways, leading to cognitive impairment and hyperactivity in mice[118]. Moreover, TANC2 directly interacts with postsynaptic density (PSD-95) and constitutes an endogenous inhibitor of mTORC1/mTORC2 complexes[118]. Moreover, it was shown that ketamine activates the mTORC1 complex by suppressing the interaction of TANC1/2 with mTOR interaction but does not affect the interaction of TANC1/2 with PSD-95[118]. Despite the still unknown physiological role of palmitoylation of TANC2 (Cys-162), its role in the biological basis of stress resilience should be considered as a potential molecular target in future studies.

In addition to the involvement of the mTOR complex in the regulation of dendritic spine structure, as well as glutamatergic neurotransmission, GSK-3-beta kinase also plays a decisive role in the development of depressive-like behavior, and the structural remodeling of dendritic spines[119–121]. In particular, our results revealed the possible role of GSK-3-beta kinase in the genesis of resilient behavior. We observed a decreased level of beta-catenin (responsible for cell survival in a Wnt-

dependent manner), suggesting the impact of GSK-3-beta/APC complex activity in the resilient group. The distinct S-PALM of two cysteines (Cys-912 and Cys-2664) in adenomatous polyposis coli (APC) protein was also observed in resilient and anhedonic mice. Due to the formation of a complex of APC and GSK-3-beta kinase, leading to the degradation of beta-catenin in the proteasome[122], the S-PALM of APC might be involved in the regulation of beta-catenin levels. Moreover, we observed a decrease in the level of the aforementioned Rictor protein in the resilient group, which was negatively correlated with the functioning of GSK-3-beta kinase[123]. Thus, we can speculate that enhanced S-PALM of APC can negatively regulate the formation of the APC/GSK-3-beta complex, decreasing the degradation of proteins, such as beta-catenin or Rictor, in the anhedonic phenotype. However interesting, these outcomes should be interpreted carefully. First, the level of beta-catenin is not regulated only by its degradation in the proteasome; therefore, the correlation between the expression of beta-catenin and the activation of the GSK-3-beta/APC complex could be misleading[122]. Concurrently, GSK-3-beta kinase activity is much more complicated than its simple involvement in the complex with APC[122]. In particular, the interplay between GSK-3-beta kinase and mTOR complexes, such as TSC-1/TSC-2, is not dependent on the GSK3-beta/APC complex but on the dephosphorylation of GSK-3-beta (Ser-9)[122,124]. Therefore, properly understanding the role of GSK-3-beta kinase in resilient and anhedonic mice requires more profound studies with complex profiling of the phosphorylation of synaptic proteins. Despite the unclear role of GSK-3-beta kinase in the decreased level of beta-catenin in the resilient phenotype, the role of this protein in the development of stress resilience is still interesting. Vidal et al. showed that inhibition of beta-catenin in GLAST-expressing cells lead to the development of depressive-like behavior while its stabilization led to a resilient state in a model of chronic exposure to corticosterone[125]. Therefore, the decreased level of beta-catenin in the hippocampus of resilient animals should be considered in the context of other signaling pathways because, as we showed, different cellular events underlie stress resilience and depressive-like behavior. Additionally, beta-catenin is a positive regulator of the transcription of MMP-9[126]; therefore, the decreased level of beta-catenin may be directly related to the unchanged activity of MMP-9 in resilient mice. Moreover, the differences in MMP-9 activity between resilient and anhedonic animals might also be explained by the lower expression levels of epithelial discoidin domain-containing receptor -1 (DDR1) in the resilient group than in the controls and anhedonic mice. The DDR1 is a unique receptor tyrosine kinase that binds to collagens, and its main role is in cell attachment to the

extracellular matrix by inducing the activity of the extracellular effectors therein MMP-2, MMP-7, and MMP-9[127].

MMP-9 is extracellularly released upon NMDAR activation under stressful conditions[72], and controls GluA1-AMPA receptor surface distribution[69]. However, our proteomic analysis of synaptic proteins did not show alterations in the expression profile of NMDA or AMPA receptors. Nevertheless, the NMDAR and AMPA receptor subunits revealed alterations in S-PALM following chronic stress. In particular, we observed increased levels of the palmitoylation of the GluA1 subunit of AMPA receptors at two cysteines (Cys-601 and Cys844). As previously reported, palmitoylation of these cysteine residues increases the anchoring of the receptor GluA1 subunit to the Golgi apparatus and inhibits the interaction between the subunit and the synaptic 41N protein, affecting glutamatergic transmission[128,129]. Increased palmitoylation of the Cys-202 residue of the GDP dissociation inhibitor-1 (GDI-1) exclusively in the anhedonic group may also indirectly regulate the turnover of AMPA receptors anchored to dendritic spines and may explain the observed decrease in spine density. It was shown previously[130,131] that the interactions of GDI-1 with the Rab family proteins are responsible for maintaining equilibrium between exocytosis and endocytosis through LTP. Unfortunately, the physiological role of Cys-202 palmitoylation of GDI-1 remains unknown. We also observed an increased level of palmitoylation of two cysteines (Cys-954 and Cys-1173) in the cytoplasmic domain of the GluN2B subunit in the anhedonic group. However, the physiological role of these GluN2B modifications has also not been described. Nevertheless, the differences in the functional readout of AMPA and NMDA receptors upon chronic stress could also be explained by the fact that palmitoylation is not the only posttranslational modification that occurs at the synapse. Several serine residues in the GluA1-A4 subunits of the AMPA receptor, as well as the GluN2B subunit, undergo phosphorylation, affecting receptor trafficking, conductance, and the frequency of the channel opening[132–134]. Therefore, the interplay between the expression, palmitoylation, phosphorylation, and ubiquitination of synaptic proteins produces a functional effect. Nevertheless, the diverse palmitoylation of AMPA and NMDA receptor subunits along with GDI-1 suggests that LTP and learning and memory might be differentially affected in resilient and anhedonic animals. Whether and how these processes are manifested within behavioral groups is a matter of further study.

In conclusion, we demonstrated that stress-resilient behavior in adult animals is a dynamically regulated process accompanied by a set of unique functional, proteomic and morphological features in the brain. In particular, we have shown that the most robust synaptic alterations underlying stress resilience are associated with the structure of dendritic spines and postsynaptic intracellular signaling pathways in the hippocampus. At the cellular level, these differences might be triggered by MMP-9 activity and/or S-PALM of synaptic proteins and translated into the regulation of synaptic receptors. However, further studies are required to indicate the chemical kinetics of these processes and their role in the behavioral stress response.

MATERIALS AND METHODS

Animals

Ten-week-old male C57BL6J mice (Medical University of Bialystok, Poland) were individually housed under a reverse 12/12 h light/dark cycle (lights on at 8:00 PM) with food and water available *ad libitum*. Male 12-week-old CD1 mice (Janvier Labs, France) were used as resident intruders in the social defeat stress procedure and kept with the stressed C57BL6J mice in the same animal room. Male 12-week-old Wistar rats (Mossakowski Medcal Research Institute, Polish Academy of Sciences, Warsaw, Poland) were used for predator stress. All animal procedures were performed according to the guidelines of the Polish Ethical Committee on Animal Research (permission no. 132/2016, 2011/2020, 203/2021, 204/2021).

Mouse Model of Stress Resilience based on Chronic Unpredictable Stress (CUS)

To evaluate depressive-like behavior in the mouse model of, we used the chronic unpredictable stress paradigm (CUS) and behavioral evaluation as we described previously[32,74]. Before CUS, C57BL/6J mice were subjected to 2 weeks of room acclimatization, consisting of 1 week of handling under a reverse 12/12 h light/dark cycle. Mice were weighed and their baseline sucrose preference (SPT0) was measured before the CUS procedure. Then, based on their baseline parameters, mice were assigned to a control and stress group housed in two separate rooms. The 2-week CUS protocol consisted of 2 out of 3 different types of stressors chosen in a semirandom manner and applied daily during the dark phase under red light in the following sequence of restraint stress, tail suspension, and social defeat stress, with an intersession of at least 3 h. During each light phase during the stress protocol, the mice were exposed to a rat. To stabilize

glucocorticoid levels after the last exposure to a stressor, the mice were left undisturbed overnight before beginning the sucrose preference test. Thus, 16 h after the last stressor, the mice underwent a sucrose preference test (SPT1), resulting in the determination of sucrose preference 24 h after the last stressor, and thereafter, the body weight measurements and the forced swim test were performed. All mice were sacrificed 12-16 h after the behavioral evaluation (36-38 h after the last stressor). To correlate the molecular, functional, and structural readouts of excitatory synaptic plasticity in the hippocampus in relation to animal behavior, two independent CUS experiments were performed in which within each animal, one hippocampus was subjected to synaptoneurosome isolation (mass spectrometry analysis) or DiI labeling (dendritic spine imaging), and the second hippocampus was subjected to electrophysiology. The experimental design is outlined in Figure 1A.

Restraint stress: The mice were placed inside a plastic tube (26 mm internal diameter) for 2 h during the dark phase.

Tail suspension stress: The mice were subjected to the tail suspension procedure by being hanged from the tails with adhesive tape for 40 min during the dark phase. To prevent the mice from climbing their tails, plastic cylinders (4 cm x 0.5 cm) were placed at the base of their tails.

Social defeat stress: During each 30 min social defeat session performed in the dark phase, aggressive CD1 animals were placed in the home cages of C57BL/6J mice in the stress group. CD1 aggressive mice were selected as the CD1 mice that attacked C57BL6J mice in less than 60 s without injuring them. During each session, the C57BL6J mice exhibited signs of social defeat stress, such as a flight response, submissive posture, and audible vocalization. If the mice in the stress group did not display signs of social defeat stress, then the CD1 mouse was changed to another CD1 mouse. In rare cases of physical harm that occurred between pairs of mice, aggressive CD1 individuals were immediately removed from the cage of the C57BL6J resident mice.

Predator stress: The mice were individually introduced into transparent, well-ventilated cylinders (15 cm x 8 cm) with food and bedding. The cylinders were then placed for 12 h (08:00 P.M.–08:00 A.M.) into a rat home cage that contained a rat during the light phase. For the rest of the day (08:00 A.M. –08:00 P.M.), the mice and rats were housed in their home cages in the same experimental room.

Behavioral Tests

Sucrose preference test (SPT)

Mice were given free-choice access to 1% sucrose solution and water that were provided in identical bottles for 8 h during the dark phase under a reverse light dark cycle. The percentage of sucrose preference was calculated as follows:

$$\text{Sucrose Preference} = [\text{Weight}_{\text{Sucrose_solution}} / (\text{Weight}_{\text{Sucrose_solution}} + \text{Weight}_{\text{Water}})] * 100\%$$

The consumption of water and sucrose solution was estimated simultaneously in the control and experimental groups by weighing the bottles. To eliminate possible bias from side preference, the positions of the bottles were changed after 4 h of the test. Twenty-four hours before the baseline sucrose preference test performed before the CUS procedure (SPT0), 2.5% sucrose solution was given to all animals for 2 h to prevent the possible effects of taste neophobia. The other conditions of the test were performed as previously described[32,74,103,104]. Sucrose preference after CUS (SPT1) values of <70.7% in mice in the stress group, measured 24 h after the last stressor, was the criterion for "anhedonia", defined by the difference between the control and stressed groups >2xSD. Anhedonic mice were previously shown to display depressive-like behavior[103,104]. None of the control animals exhibited <70.7% sucrose preference in SPT1. Stressed mice with sucrose preference >70.7% at the end of the CUS experiment were defined as resilient animals. The SPT evaluation before (SPT0) and after CUS (SPT1) is outlined in Figure 1B.

Forced swim test (FST)

Each mouse was placed into a cylindrical glass containers (20 cm x 40 cm) filled with warm water (~27 ^{o}C) for a 6 min swimming session. The test was conducted under red light during the dark phase of the light/dark cycle after 1 h of room acclimatization where the behavioral test was performed. The sum of the floating time during the last 4 min was measured by visual scoring offline and defined as the time spent immobile.

Drug administration in CUS

Experiments with the CUS procedure and a single intraperitoneal drug administration of (R, S)-ketamine hydrochloride (3 mg/kg body weight; Biowet Pulawy, Poland) or saline (0.9% sodium chloride) were performed using a separate CUS model with an additional behavioral evaluation of

the antidepressive effect of ketamine using the sucrose preference test (SPT2) 24 h after intraperitoneal ketamine administration. Ketamine or saline was administered to control and stressed (anhedonic and resilient) animals after the standard sucrose preference test (SPT1) following the CUS procedure. The experimental design and results are outlined in *Supplementary Figure 1*. The purity of the administered drugs was determined using UPLC–MS analysis, as presented in *Supplementary Figure 3*.

Acute Brain Slice Electrophysiology

Acute hippocampal brain slices were obtained from control, anhedonic, and resilient mice (N at least 5 mice/group) according to the protocol described previously[135]. The hippocampi from one hemisphere were dissected and cut into 350 µm thick slices using a vibratome (VT1200S, Leica, Germany) in ice-cold buffer that contained 75 mM sucrose, 87 mM NaCl, 2.5 mM KCl, 1.25 mM NaH_2PO_4, 25 mM $NaHCO_3$, 0.5 mM $CaCl_2$, 10 mM $MgSO_4*7H_2O$, and 20 mM glucose, pH 7.4. Slices were recovered in the same solution for 15 min (32 °C) and were subsequently stored in oxygenated (95% O_2, 5% CO_2) artificial cerebrospinal fluid (aCSF) that contained 125 mM NaCl, 25 mM $NaHCO_3$, 2.6 mM KCl, 1.25 mM NaH_2PO_4, 2.0 mM $CaCl_2$, and 20 mM glucose, pH 7.4. Recordings were made in aCSF after 2 hours of slice recovery. Schaeffer collateral axons were stimulated with a concentric bipolar electrode (0.1 Hz, 0.3 ms, FHC, Bowdoin, ME USA). Compound AMPAR- and NMDAR-mediated fEPSPs were recorded with glass micropipettes that were filled with aCSF (1-3 M Ω resistance) in the Stratum Radiatum of the CA1 region of the hippocampus. NMDAR-mediated signals were isolated from compound fEPSPs with the AMPA/kainate receptor antagonist DNQX (20 µM) and L-type calcium channel blocker nifedipine (20 µM) in Mg^{2+}-free solutions, as described previously[135]. At the end of each recording, the NMDAR antagonist APV (50 µM) was used to confirm the origin of the recorded fEPSPs. Input–output (I–O) relationships were built for fEPSPs amplitudes upon monotonically increasing the stimuli in the range of 0–300 µA (13 points, applied once at 0.1 Hz). Baseline stimulation was set at 0.1 Hz, and for baseline and paired-pulse stimulation protocols (interstimulus interval 25 ms), the stimulation strength was set to 40% of the maximum fEPSP amplitude. For better data visualization, the input–output curves shown in Figure 3A were fitted with Equation (1):

$y(x) = an\ \mathrm{arctg}\frac{x}{b}$.

Once the data were fitted, more complicated dependences, e.g., fEPSP amplitude vs. fiber volley amplitude, were recovered by combining the fit in the form of z(x) (with parameters a, b) with an inverse of the relation (1) in the form of x(y), with $x = b' \mathrm{tg}\frac{y}{a'}$, which led to $z = a \,\mathrm{arctg}\, \frac{b'}{b} \mathrm{tg}\frac{y}{a'}$ (Figure 3B-C).

The statistical significance of the differences between the stimulation current, fiber volley amplitudes and fEPSPs, $V(I)$, obtained from the electrophysiological experiments (Figure 3B-C), was determined by Monte Carlo methods. The p values were calculated using a randomization approach[136]. In the first step, we quantified the differences between the measured $V^A(I_i)$ and $V^B(I_i)$ curves using the L_2 norm, defined as

$$L_2 = \sqrt{\sum_{i=0}^{N}(V^A(I_i) - V^B(I_i))^2},$$

where I_i is the stimulation current for the *i*-th measurement point and *N* is the total number of the measurement points. To compute the p values, we created the null-hypothesis ensemble, using the subject randomization. The p value for the difference between two $V(I)$ curves was calculated as

$$p_{value} = \frac{\sum_{j=1}^{B} F(L_{2\,j} \geq L_{2\,true})}{B+1},$$

where *F* is the indicator function that takes the value one when its argument is true and zero when it is false, $L_{2\,j}$ is the L_2 norm for the -*j*th element of the null-hypothesis ensemble, $L_{2\,true}$ is the actual value of L_2 for the analyzed $V(I)$ curves, and *B* is the number of randomizations (we used *B*=1000). All of the drugs were obtained from Sigma–Aldrich (Poland) and Tocris (UK). The electrophysiology data were analyzed using AxoGraphX software as described previously[135].

Synaptoneurosome

After euthanasia by cervical dislocation, the mice were decapitated, and hippocampi were removed and homogenized with a Dounce homogenizer in 3 mL of buffer A (5 mM HEPES (pH 7.4), 0.32 M sucrose, 0.2 mM ethylenediaminetetraacetic acid (EDTA), 50 mM N-ethylmaleimide (NEM), and protease inhibitor cocktail. Nuclei and cell debris were pelleted by 5 min centrifugation at 2 500 × g. The supernatant was then centrifuged at 12 000 × g for 5 min. The obtained pellet fraction was layered over a discontinuous Ficoll (Sigma Aldrich) gradient (4%, 6%, and 13%) and centrifuged at 70 000 × g for 45 min. The synaptoneurosomal fraction was collected in buffer A

and centrifuged at 20 000 × g for 20 min. The pellet corresponded to the synaptoneurosomes fraction. Purified synaptoneurosomes were obtained from the hippocampus collected from one hemisphere of control, anhedonic, resilient animals (N mice/group=5) and subjected to mass spectrometry analysis as described previously[85]. The obtained synaptoneurosomal fraction was visualized using electron microscopy and is presented in the *Supplementary Figure 2*.

Mass Spectrometry

The S-PALM or total protein peptide mixture (20 µL) was applied to the nanoACQUITY UPLC Trapping Column (Waters, 186003514) using water containing 0.1% formic acid as the mobile phase and transferred to the nanoACQUITY UPLC BEH C18 Column (75 µm inner diameter; 250 mm long, Waters 186003545) using an acetonitrile gradient in the presence of 0.1% formic acid with a flow rate of 250 nL/min. The column outlet was directly coupled to the ion source of the Thermo Orbitrap Elite mass spectrometer (Thermo Electron Corp., San Jose, CA, USA) working in the regime of data-dependent MS to MS/MS switch. HCD fragmentation was used. All MS runs were separated by blank runs to reduce the carry-over of peptides from previous samples. The results of measurements were processed using Mascot-Distiller 2.7.1 software (MatrixScience, London, UK, on-site license). The Mascot search engine (version 2.7.1) was used to compare data against the UniProtKB/Swiss-Prot database (Swissprot 2020_02; 16,905 sequences). The search parameters were set to the following: taxonomy (*Mus musculus*), variable modifications – cysteine carbamidomethylation or N-malemideidation, methionine oxidation, peptide tolerance (5 ppm), fragment mass tolerance (5 ppm). Enzyme specificity was set for trypsin with one missed or nonspecific cleavage permitted. The mass calibration and data filtering described above were also carried out. The lists of the peptide sequences (SPL) that were identified in all of the LC–MS/MS runs from synaptoneurosomal fractions were merged into one peptide list using MascotScan software (http://proteom.ibb.waw.pl/mscan/, accessed on 9 April 2021). The SPL consists of sequences of peptides with Mascot scores exceeding the threshold value corresponding to a 5% expectation value and FDR of 1% calculated by the Mascot procedure. For proteome quantitative analysis, peptide intensities were determined as the surface of the isotopic envelope of the tagged isotopic envelopes. Before the analysis, quantitative values were normalized with LOWESS as described previously[85].

Functional Bioinformatics Analysis of Mass Spectrometry Data

For integrative analysis, we used ClueGO software to observe differential proteins involved in the GO terms. The input list of proteins for each GO analysis was distinguished on the basis of proteomic data analysis and Venn diagram analysis. The lists of proteins are grouped in *Supplementary Tables 1-2* included in the *Supplementary Materials*. Proteins were analyzed with ClueGO v2.6.4/CluePedia v1.6.5 to obtain complete Gene Ontological terms (GO) from our datasets. ClueGO integrates GO terms and creates an organized GO/pathway term network. The statistical test used for the node enrichment was based on a right-sided hypergeometric option with a Benjamini–Hochberg correction and kappa score of 0.5. As a reference set for term enrichment calculations, we utilized genes from the *Mus musculus* genome (NCBI unique Gene identifiers). GO enrichment was conducted for different sets of proteins, and p values <0.05 were considered to be significant. ClueGO results are grouped in Figure 5.

UPLC–MS analysis of ketamine hydrochloride samples

The identity and purity of the ketamine used in the study was assessed via ultra-performance liquid chromatography-tandem mass spectrometry (UPLC–MS) on a Waters TQD spectrometer combined with a UPLC Acquity H-Class with a PDA eLambda detector. A 50-µL sample from the stock solution was diluted with UPLC grade water (950 µL) and analyzed using a Waters Acquity UPLC BEH C18 chromatographic column (1.7 µm, 2.1x100 mm) under the following conditions: temperature, 40 °C; flow, 0.300 mL/min; and injection volume, 1.0 µL. The mass spectra were recorded using positive mode electrospray ionization (ESI+), and the chromatograms were recorded with UV detection in the 190-300 nm range. The following gradient conditions were used: 80% phase A (water + 0.1% formic acid) and 20% phase B (acetonitrile + 0.1% formic acid) to 100% phase B (acetonitrile + 0.1% formic acid) over 3.0 min, hold at 100% phase B until 3.5 min, return to initial conditions by 4.0 min, and hold for an additional 2.0 min. The total length of the analysis was 6.0 min.

DiI Staining of Brain Slices and Morphometric Analysis of Dendritic Spines

To visualize changes in the structure of dendritic spines, 1,10-dioctadecyl-3,3,3,30-tetramethylindocarbocyanine perchlorate (DiI) staining was performed on one brain hemisphere fixed by incubation for 1 h in 1.5% paraformaldehyde. The hemispheres were sliced using a Leica

vibratome. Slices (140 µm thick) containing hippocampal structures were allowed to recover for at least 1.5 h at room temperature. Random cell labeling was performed using 1.6 µm tungsten particles (Bio–Rad, Hercules, CA, USA) that were coated with a propelled lipophilic fluorescent dye (DiI; Invitrogen) delivered to the cells by gene gun (Bio–Rad) bombardment. Images of hippocampal neurons covered with dendritic spines were acquired under 561 nm fluorescent illumination using a confocal microscope Zeiss LSM800 (63× objective, 1.4 NA) at a pixel resolution of 1024 x 1024 with a 2.4 x zoom, resulting in a 0.07 µm pixel size. The analysis of dendritic spine structure and calculation of changes in spine parameters were performed as described previously[32,63,74]. The images that were acquired from the brain slices were processed using ImageJ software (National Institutes of Health, Bethesda, MD, USA) and analyzed semiautomatically using custom-written SpineMagick software (patent no. WO/2013/021001). The analyzed dendritic spines belonged to secondary and ternary dendrites to reduce possible differences in spine morphology caused by the location of spines on dendrites with different ranks. To quantify the changes in spine shape, we analyzed the relative changes in the spine length-to-head-width ratio (the scale-free parameter). The spine length was determined by measuring the curvilinear length along a fitted virtual skeleton of the spine. The fitting procedure was performed by looking for a curve along which integrated fluorescence was at a maximum. Head width was defined as the diameter of the largest spine section while excluding the bottom part of the spine (1/3 of the spine length adjacent to the dendrite). Dendritic segments of 5 animals per group (70-93 cells/group) were morphologically analyzed resulting in CTR N_{spines}=7 735, $N_{dendrites}$=116; ANH N_{spines}=7 918, $N_{dendrites}$=120; RES N_{spines}=7 026 $N_{dendrites}$=107. To assess dendritic length for spine density analysis, we measured curvilinear length along the analyzed dendritic segment, which was obtained by fitting an n-order polynomial resulting in $CTR_{dendritic\ length}$= 23 795.67 µm, $ANH_{dendritic\ length}$= 27 179.45 µm, and $RES_{dendritic\ length}$= 21 996.42 µm. The spine number was counted manually by a trained neurobiologist in ImageJ software. The statistical analysis was performed using nested analysis of variance. The distributions of spine parameters for spine density, length/head width, and area for the control, anhedonic and resilient groups are presented in *Supplementary Figure 4*.

Gel zymography

The gel zymography procedure was performed as we described previously[64,74] in a separate cohort of control, anhedonic and resilient animals. MMPs were extracted from the hippocampi via affinity

chromatography using gelatin-Sepharose 4B (GE Healthcare) as previously described with slight modifications[137]. The tissues were homogenized in working buffer consisting of 50 mM Tris-HCl, pH 7.5, 150 mM NaCl, 5 mM $CaCl_2$, and 1% Triton X-100 containing 0.02% NaN_3. The homogenates were centrifuged for 15 min at 4 °C and 12 000 × g. A 5-μL aliquot of the recovered supernatant was saved and assayed for total protein levels with a PierceTM BCA Protein Assay Kit. Equal amounts of proteins (500-1 000 μg) were incubated with gelatin-Sepharose 4B at 4 °C overnight with agitation. Then, after centrifugation for 2 min at 4 °C and 6 000 × g, supernatant was removed, and the gelatin-Sepharose pellets were incubated at 4 °C for 2 h with elution buffer consisting of the working buffer plus 10% DMSO. The samples were mixed with 4× sample buffer (0.2 M Tris-HCl, pH 6.8, 8% SDS, 40% glycerol, and 0.008% bromophenol blue), loaded on an 8% polyacrylamide gel copolymerized with 1 mg/mL gelatin as a substrate and run for 3 h at 90 V. After electrophoresis, the SDS was removed from the gels by washing twice with zymogram renaturating buffer (2.5% Triton X-100, 30 min each), and the gels were then incubated at 37 °C in a developing buffer containing 50 mM Tris-HCl, pH 7.5, 1% Triton X-100, 10 mM $CaCl_2$, 0.02% NaN3, and 1 μM $ZnCl_2$ for 24-96 NaN_3, and 1 μM $ZnCl_2$ for 24-96 h. Following incubation, the gels were stained with Coomassie Blue R-250 and then destained appropriately. ImageJ software was used to measure the mean optical densities of the MMP-9 and MMP-2 bands.

CDC42 pulldown

Activated CDC42 was pulled down as previously described[138,139]. Briefly, brain tissues were homogenized in assay buffer comprising of 25 mM HEPES, pH 7.5, 150 mM NaCl, 1% Nonidet P-40, 10 mM MgCl 2, 1 mM ethylenediaminetetraacetic acid (EDTA), and 2% glycerol. The homogenates were centrifuged for 10 min at 4 °C and 14 000 × g. A 5-μL aliquot of the recovered supernatant was saved and assayed for total protein levels by a Pierce™ BCA Protein Assay Kit. After the samples were diluted to equal protein concentrations, an aliquot of each lysate was used to measure the total expression of CDC42 by Western blotting. The remainder of each sample was incubated with GST-PAK-PBD (Cell Biolabs) fusion protein conjugated to glutathione beads at 4 °C overnight and then washed three times with the assay buffer. GST-PAK-PBD-bound CDC42 was analyzed by sodium dodecyl sulfate–polyacrylamide gel electrophoresis (SDS PAGE) and subsequently immunoblotted with a CDC42-specific antibody.

Western blot analysis

Protein samples were separated by SDS–PAGE and transferred to polyvinylidene difluoride membranes (Immobilon-P, Millipore). The membranes were then blocked with 10% nonfat milk in Tris-buffered saline with 0.1% Tween 20 (TBST). After blocking, the membranes were incubated overnight at 4 °C with anti-CDC42 (1:500; 11A11, Cell Signaling) diluted in 3% bovine serum albumin in TBST and anti-GAPDH (1:10 000; MAB374, Millipore) diluted in 5% nonfat milk in TBST. The blots were washed three times with TBST and then incubated for 1 h with a peroxidase-conjugated secondary antibody diluted 1:5 000 in TBST containing 5% nonfat milk. After washing, the bands were detected using the SuperSignal West Femto Maximum Sensitivity Substrate (for CDC42 detection) or SuperSignal West Pico PLUS Chemiluminescent Substrate (for GAPDH detection) (Thermo Fisher Scientific).

Statistical Analysis

Statistical analysis was performed using GraphPad Prism8 software (GraphPad, San Diego, CA, USA). One-way or two-way analysis of variance (one-way or two-way ANOVA) followed by post hoc tests was used for multiple comparisons to identify significant differences between experimental groups. In the case of unequal variances, the Welch correction was applied. If the data were not normally distributed, the Mann–Whitney test was used. Behavioral data were analyzed using one-way ANOVA followed by the Bonferroni or Tukey post hoc tests. For the statistical analysis of the structural plasticity of dendritic spines (density and morphology), we used nested-ANOVA statistics, including the number of animals and the number of cells/spines analyzed per behavioral group. The nested-ANOVA statistics were performed with R 4.1.1, the language and environment for statistical computing (R Foundation for Statistical Computing, Vienna, Austria). The zymograms were quantitatively analyzed by the sum of replicates (each data point on a replicate is divided by the sum of the values of all data points in that replicate)[140]. A p value of <0.05 was considered statistically significant for all tests except for mass spectrometry results in which <0.01 was used. The data are presented as the mean value ± SEM. All analyses were performed in a blinded manner.

Data availability

All data supporting the findings of this study are available within the article or are available from the corresponding author upon reasonable request. The mass spectrometry proteomics data have been deposited to the ProteomeXchange Consortium via the PRIDE partner repository with the dataset identifier PXD026590.

Author contributions

Conceived the study: JW and EB. Experimental design: JW, EB, AK, MZK, MM, TW. Performed the experiments: EB, AK, TW, MM, MZK, KB, KHO, ADW, MB. In detail: chronic unpredictable stress model (CUS): EB, AK, KB, KHO, AW, and SA; behavioral tests: EB, AK, BP; drug administration: EB, BP; isolation of hippocampal synaptoneurosomes: MZK, IF; mass spectrometry: MZK; electrophysiology: TW; DiI labeling of hippocampal slices: MM, MR, EB; image acquisition: MM, MR; morphometric analysis of dendritic spines: EB; gel zymography: MB; pull down: MB; LC–MS analysis: AH; analyzed the data: EB, AK, MZK, JW, JM, MB; statistical analysis: BR, RW, PS, EB. Contributed reagents/materials/analysis tools/data interpretation: JW, EB, MB, BR, RKF, BP, BS, KR, JD, PJ, KR. Wrote the paper: EB, JW, BP. All authors corrected and accepted the manuscript.

Acknowledgments

This work was supported by grants from a National Science Centre (2021/41/B/NZ4/02603, UMO-2017/26/E/NZ4/00637 and UMO-2017/27/N/NZ3/02417). TW was supported by a National Science Centre (UMO-2019/34/E/NZ4/00387). MB, JM, and BP were supported by a National Science Centre grant (UMO- 2019/35/D/NZ4/02042). KB was supported by a National Science Centre (UMO-2020/37/N/NZ4/02869). IF was supported by a National Science Centre (UMO-2015/19/B/NZ3/01376). SA was founded from the European Union's Horizon 2020 research and innovation program under a Marie Skłodowska-Curie grant (agreement no. 665735).

Declaration of Interests

The authors declare that they have no conflicts of interest.

References

1. Suresh, S. *Fatigue of Materials*. (Cambridge University Press, 1998).
2. Kakani, S. L. *Material Science*. (New Age International (P) Ltd., Publishers, 2004).
3. Hassler, U. & Kohler, N. Resilience in the built environment. *Build. Res. Inf.* **42**, 119–129 (2014).
4. Weichselgartner, J. & Kelman, I. Geographies of resilience: Challenges and opportunities of a descriptive concept. *Prog. Hum. Geogr.* **39**, 249–267 (2015).
5. Rankenberg, T. *et al.* Age-Dependent Abiotic Stress Resilience in Plants. *Trends Plant Sci.* **26**, 692–705 (2021).
6. Pushpalal, D. & Suzuki, A. A New Methodology for Measuring Tsunami Resilience Using Theory of Springs. *Geosciences* **10**, 469 (2020).
7. Adger, W. N. Social and ecological resilience: are they related? *Prog. Hum. Geogr.* **24**, 347–364 (2000).
8. Bryan, C., O'Shea, D. & MacIntyre, T. Stressing the relevance of resilience: A systematic review of resilience across the domains of sport and work. *Int. Rev. Sport Exerc. Psychol.* **12**, 70–111 (2019).
9. Plummer, R. & Armitage, D. A resilience-based framework for evaluating adaptive co-management: Linking ecology, economics and society in a complex world. *Ecol. Econ.* **61**, 62–74 (2007).
10. Richter-Levin, G. & Sandi, C. Title: "Labels Matter: Is it stress or is it Trauma?" *Transl. Psychiatry* **11**, 1–9 (2021).
11. Stern, Y. *et al.* Whitepaper: Defining and investigating cognitive reserve, brain reserve, and brain maintenance. *Alzheimers Dement.* **16**, 1305–1311 (2020).
12. Richardson, G. E. The metatheory of resilience and resiliency. *J. Clin. Psychol.* **58**, 307–321 (2002).
13. Den Hartigh, R. J. R. & Hill, Y. Conceptualizing and measuring psychological resilience: What can we learn from physics? *New Ideas Psychol.* **66**, 100934 (2022).
14. Fletcher, D. & Sarkar, M. Psychological Resilience. *Eur. Psychol.* **18**, 12–23 (2013).
15. Southwick, S. M., Bonanno, G. A., Masten, A. S., Panter-Brick, C. & Yehuda, R. Resilience definitions, theory, and challenges: interdisciplinary perspectives. *Eur. J. Psychotraumatology* **5**, (2014).
16. Arenaza-Urquijo, E. M. & Vemuri, P. Resistance vs resilience to Alzheimer disease. *Neurology* **90**, 695–703 (2018).
17. Hess, J. L. *et al.* A polygenic resilience score moderates the genetic risk for schizophrenia. *Mol. Psychiatry* **26**, 800–815 (2021).
18. Davydov, D. M., Stewart, R., Ritchie, K. & Chaudieu, I. Resilience and mental health. *Clin. Psychol. Rev.* **30**, 479–495 (2010).
19. Kane, C. *et al.* Clinical factors influencing resilience in patients with anorexia nervosa. *Neuropsychiatr. Dis. Treat.* **15**, 391–395 (2019).

20. Y, M., F, W. & B, F.-A. Resilience research in schizophrenia: a review of recent developments. *Curr. Opin. Psychiatry* **29**, (2016).
21. Franklin, T. B., Saab, B. J. & Mansuy, I. M. Neural mechanisms of stress resilience and vulnerability. *Neuron* **75**, 747–761 (2012).
22. Wu, G. *et al.* Understanding resilience. *Front. Behav. Neurosci.* **7**, 10 (2013).
23. Rakesh, G. *et al.* Resilience as a Translational Endpoint in the Treatment of PTSD. *Mol. Psychiatry* **24**, 1268–1283 (2019).
24. Maul, S. *et al.* Genetics of resilience: Implications from genome-wide association studies and candidate genes of the stress response system in posttraumatic stress disorder and depression. *Am. J. Med. Genet. B Neuropsychiatr. Genet.* **183**, 77–94 (2020).
25. Peña, C. J., Nestler, E. J. & Bagot, R. C. Environmental Programming of Susceptibility and Resilience to Stress in Adulthood in Male Mice. *Front. Behav. Neurosci.* **13**, (2019).
26. Krishnan, V. *et al.* Molecular adaptations underlying susceptibility and resistance to social defeat in brain reward regions. *Cell* **131**, 391–404 (2007).
27. Isingrini, E. *et al.* Resilience to chronic stress is mediated by noradrenergic regulation of dopamine neurons. *Nat. Neurosci.* **19**, 560–563 (2016).
28. Cathomas, F., Murrough, J. W., Nestler, E. J., Han, M.-H. & Russo, S. J. Neurobiology of Resilience: Interface Between Mind and Body. *Biol. Psychiatry* **86**, 410–420 (2019).
29. Highland, J. N., Zanos, P., Georgiou, P. & Gould, T. D. Group II metabotropic glutamate receptor blockade promotes stress resilience in mice. *Neuropsychopharmacology* **44**, 1788–1796 (2019).
30. Friedman, A. K. *et al.* KCNQ channel openers reverse depressive symptoms via an active resilience mechanism. *Nat. Commun.* **7**, 11671 (2016).
31. Stainton, A. *et al.* Resilience as a multimodal dynamic process. *Early Interv. Psychiatry* **13**, 725–732 (2019).
32. Krzystyniak, A. *et al.* Prophylactic Ketamine Treatment Promotes Resilience to Chronic Stress and Accelerates Recovery: Correlation with Changes in Synaptic Plasticity in the CA3 Subregion of the Hippocampus. *Int. J. Mol. Sci.* **20**, (2019).
33. Brachman, R. A. *et al.* Ketamine as a Prophylactic Against Stress-Induced Depressive-like Behavior. *Biol. Psychiatry* **79**, 776–786 (2016).
34. Okine, T., Shepard, R., Lemanski, E. & Coutellier, L. Sex Differences in the Sustained Effects of Ketamine on Resilience to Chronic Stress. *Front. Behav. Neurosci.* **14**, (2020).
35. Camargo, A., Dalmagro, A. P., Wolin, I. A. V., Kaster, M. P. & Rodrigues, A. L. S. The resilient phenotype elicited by ketamine against inflammatory stressors-induced depressive-like behavior is associated with NLRP3-driven signaling pathway. *J. Psychiatr. Res.* **144**, 118–128 (2021).
36. MÉNARD, C., HODES, G. E. & RUSSO, S. J. Pathogenesis of depression: insights from human and rodent studies. *Neuroscience* **321**, 138–162 (2016).
37. Becker, M., Pinhasov, A. & Ornoy, A. Animal Models of Depression: What Can They Teach Us about the Human Disease? *Diagnostics* **11**, 123 (2021).

38. Shadrina, M., Bondarenko, E. A. & Slominsky, P. A. Genetics Factors in Major Depression Disease. *Front. Psychiatry* **9**, 334 (2018).
39. Malhi, G. S. & Mann, J. J. Depression. *The Lancet* **392**, 2299–2312 (2018).
40. Schmitt, A., Malchow, B., Hasan, A. & Falkai, P. The impact of environmental factors in severe psychiatric disorders. *Front. Neurosci.* **8**, (2014).
41. Duman, R. S., Aghajanian, G. K., Sanacora, G. & Krystal, J. H. Synaptic plasticity and depression: new insights from stress and rapid-acting antidepressants. *Nat. Med.* **22**, 238–249 (2016).
42. Logan, R. W. *et al.* Chronic Stress Induces Brain Region-Specific Alterations of Molecular Rhythms that Correlate with Depression-like Behavior in Mice. *Biol. Psychiatry* **78**, 249–258 (2015).
43. Bremner, J. D. Stress and Brain Atrophy. *CNS Neurol. Disord. Drug Targets* **5**, 503–512 (2006).
44. Castrén, E. & Monteggia, L. M. Brain-Derived Neurotrophic Factor Signaling in Depression and Antidepressant Action. *Biol. Psychiatry* **90**, 128–136 (2021).
45. MacQueen, G. & Frodl, T. The hippocampus in major depression: evidence for the convergence of the bench and bedside in psychiatric research? *Mol. Psychiatry* **16**, 252–264 (2011).
46. Filatova, E. V., Shadrina, M. I. & Slominsky, P. A. Major Depression: One Brain, One Disease, One Set of Intertwined Processes. *Cells* **10**, 1283 (2021).
47. HASLER, G. PATHOPHYSIOLOGY OF DEPRESSION: DO WE HAVE ANY SOLID EVIDENCE OF INTEREST TO CLINICIANS? *World Psychiatry* **9**, 155–161 (2010).
48. Holmes, S. E. *et al.* Lower synaptic density is associated with depression severity and network alterations. *Nat. Commun.* **10**, 1529 (2019).
49. Marsden, W. N. Synaptic plasticity in depression: Molecular, cellular and functional correlates. *Prog. Neuropsychopharmacol. Biol. Psychiatry* **43**, 168–184 (2013).
50. Price, R. B. & Duman, R. Neuroplasticity in cognitive and psychological mechanisms of depression: an integrative model. *Mol. Psychiatry* **25**, 530–543 (2020).
51. Thompson, S. M. *et al.* An excitatory synapse hypothesis of depression. *Trends Neurosci.* **38**, 279–294 (2015).
52. Autry, A. E. *et al.* NMDA receptor blockade at rest triggers rapid behavioural antidepressant responses. *Nature* **475**, 91–95 (2011).
53. Duman, R. S., Li, N., Liu, R.-J., Duric, V. & Aghajanian, G. Signaling pathways underlying the rapid antidepressant actions of ketamine. *Neuropharmacology* **62**, 35–41 (2012).
54. Treccani, G. *et al.* S-Ketamine Reverses Hippocampal Dendritic Spine Deficits in Flinders Sensitive Line Rats Within 1 h of Administration. *Mol. Neurobiol.* **56**, 7368–7379 (2019).
55. Beyeler, A. Do antidepressants restore lost synapses? *Science* **364**, 129–130 (2019).
56. Sala, C. & Segal, M. Dendritic Spines: The Locus of Structural and Functional Plasticity. *Physiol. Rev.* **94**, 141–188 (2014).
57. Tønnesen, J. & Nägerl, U. V. Dendritic Spines as Tunable Regulators of Synaptic Signals. *Front. Psychiatry* **7**, (2016).

58. Penzes, P., Cahill, M. E., Jones, K. A., VanLeeuwen, J.-E. & Woolfrey, K. M. Dendritic spine pathology in neuropsychiatric disorders. *Nat. Neurosci.* **14**, 285–293 (2011).
59. Chidambaram, S. B. *et al.* Dendritic spines: Revisiting the physiological role. *Prog. Neuropsychopharmacol. Biol. Psychiatry* **92**, 161–193 (2019).
60. Bączyńska, E., Pels, K. K., Basu, S., Włodarczyk, J. & Ruszczycki, B. Quantification of Dendritic Spines Remodeling under Physiological Stimuli and in Pathological Conditions. *Int. J. Mol. Sci.* **22**, 4053 (2021).
61. Qiao, H. *et al.* Dendritic Spines in Depression: What We Learned from Animal Models. *Neural Plast.* **2016**, 8056370 (2016).
62. Moda-Sava, R. N. *et al.* Sustained rescue of prefrontal circuit dysfunction by antidepressant-induced spine formation. *Science* **364**, (2019).
63. Magnowska, M. *et al.* Transient ECM protease activity promotes synaptic plasticity. *Sci. Rep.* **6**, 27757 (2016).
64. Bijata, M. *et al.* Synaptic Remodeling Depends on Signaling between Serotonin Receptors and the Extracellular Matrix. *Cell Rep.* **19**, 1767–1782 (2017).
65. Wiera, G. & Mozrzymas, J. W. Extracellular Metalloproteinases in the Plasticity of Excitatory and Inhibitory Synapses. *Cells* **10**, 2055 (2021).
66. Schill, Y. *et al.* Serotonin 5-HT4 receptor boosts functional maturation of dendritic spines via RhoA-dependent control of F-actin. *Commun. Biol.* **3**, 76 (2020).
67. Michaluk, P. *et al.* Influence of matrix metalloproteinase MMP-9 on dendritic spine morphology. *J. Cell Sci.* **124**, 3369–3380 (2011).
68. Szepesi, Z., Bijata, M., Ruszczycki, B., Kaczmarek, L. & Wlodarczyk, J. Matrix Metalloproteinases Regulate the Formation of Dendritic Spine Head Protrusions during Chemically Induced Long-Term Potentiation. *PLOS ONE* **8**, e63314 (2013).
69. Szepesi, Z. *et al.* Synaptically Released Matrix Metalloproteinase Activity in Control of Structural Plasticity and the Cell Surface Distribution of GluA1-AMPA Receptors. *PLOS ONE* **9**, e98274 (2014).
70. Domenici, E. *et al.* Plasma protein biomarkers for depression and schizophrenia by multi analyte profiling of case-control collections. *PloS One* **5**, e9166 (2010).
71. Rybakowski, J. K. *et al.* Increased serum matrix metalloproteinase-9 (MMP-9) levels in young patients during bipolar depression. *J. Affect. Disord.* **146**, 286–289 (2013).
72. van der Kooij, M. A. *et al.* Role for MMP-9 in stress-induced downregulation of nectin-3 in hippocampal CA1 and associated behavioural alterations. *Nat. Commun.* **5**, 4995 (2014).
73. Shibasaki, C. *et al.* Altered Serum Levels of Matrix Metalloproteinase-2, -9 in Response to Electroconvulsive Therapy for Mood Disorders. *Int. J. Neuropsychopharmacol.* **19**, pyw019 (2016).
74. Bijata, M. *et al.* Activation of the 5-HT7 receptor and MMP-9 signaling module in the hippocampal CA1 region is necessary for the development of depressive-like behavior. *Cell Rep.* **38**, 110532 (2022).

75. Zaręba-Kozioł, M., Figiel, I., Bartkowiak-Kaczmarek, A. & Włodarczyk, J. Insights Into Protein S-Palmitoylation in Synaptic Plasticity and Neurological Disorders: Potential and Limitations of Methods for Detection and Analysis. *Front. Mol. Neurosci.* **11**, 175 (2018).
76. Ji, B. & Skup, M. Roles of palmitoylation in structural long-term synaptic plasticity. *Mol. Brain* **14**, 8 (2021).
77. Piguel, N. H. *et al.* Ankyrin-G-190 palmitoylation mediates dendrite and spine morphogenesis and is altered in response to lithium. *bioRxiv* 620708 (2019) doi:10.1101/620708.
78. Mumby, S. M. Reversible palmitoylation of signaling proteins. *Curr. Opin. Cell Biol.* **9**, 148–154 (1997).
79. Milligan, G., Parenti, M. & Magee, A. I. The dynamic role of palmitoylation in signal transduction. *Trends Biochem. Sci.* **20**, 181–187 (1995).
80. Fukata, Y. & Fukata, M. Protein palmitoylation in neuronal development and synaptic plasticity. *Nat. Rev. Neurosci.* **11**, 161–175 (2010).
81. Kang, R. *et al.* Neural Palmitoyl-Proteomics Reveals Dynamic Synaptic Palmitoylation. *Nature* **456**, 904–909 (2008).
82. Jeyifous, O. *et al.* Palmitoylation regulates glutamate receptor distributions in postsynaptic densities through control of PSD95 conformation and orientation. *Proc. Natl. Acad. Sci.* **113**, E8482–E8491 (2016).
83. Retana-Márquez, S. *et al.* Body weight gain and diurnal differences of corticosterone changes in response to acute and chronic stress in rats. *Psychoneuroendocrinology* **28**, 207–227 (2003).
84. Tamashiro, K. L., Sakai, R. R., Shively, C. A., Karatsoreos, I. N. & Reagan, L. P. Chronic stress, metabolism, and metabolic syndrome. *Stress* **14**, 468–474 (2011).
85. Zareba-Koziol, M. *et al.* Stress-induced Changes in the S-palmitoylation and S-nitrosylation of Synaptic Proteins. *Mol. Cell. Proteomics MCP* **18**, 1916–1938 (2019).
86. Zaręba-Kozioł, M., Szwajda, A., Dadlez, M., Wysłouch-Cieszyńska, A. & Lalowski, M. Global analysis of S-nitrosylation sites in the wild type (APP) transgenic mouse brain-clues for synaptic pathology. *Mol. Cell. Proteomics MCP* **13**, 2288–2305 (2014).
87. Brzdąk, P., Włodarczyk, J., Mozrzymas, J. W. & Wójtowicz, T. Matrix Metalloprotease 3 Activity Supports Hippocampal EPSP-to-Spike Plasticity Following Patterned Neuronal Activity via the Regulation of NMDAR Function and Calcium Flux. *Mol. Neurobiol.* **54**, 804–816 (2017).
88. Kim, E., Owen, B., Holmes, W. R. & Grover, L. M. Decreased afferent excitability contributes to synaptic depression during high-frequency stimulation in hippocampal area CA1. *J. Neurophysiol.* **108**, 1965–1976 (2012).
89. Brzdak, P. *et al.* Synaptic Potentiation at Basal and Apical Dendrites of Hippocampal Pyramidal Neurons Involves Activation of a Distinct Set of Extracellular and Intracellular Molecular Cues. *Cereb. Cortex N. Y. N 1991* **29**, 283–304 (2019).
90. Eskandari, F., Salimi, M., Hedayati, M. & Zardooz, H. Maternal separation induced resilience to depression and spatial memory deficit despite intensifying hippocampal inflammatory responses to chronic social defeat stress in young adult male rats. *Behav. Brain Res.* 113810 (2022) doi:10.1016/j.bbr.2022.113810.

91. Lotan, A. *et al.* Neural mechanisms underlying stress resilience in Ahi1 knockout mice: relevance to neuropsychiatric disorders. *Mol. Psychiatry* **19**, 243–252 (2014).
92. Henry, F. E., Hockeimer, W., Chen, A., Mysore, S. P. & Sutton, M. A. Mechanistic target of rapamycin is necessary for changes in dendritic spine morphology associated with long-term potentiation. *Mol. Brain* **10**, 50 (2017).
93. Li, N. *et al.* mTOR-dependent synapse formation underlies the rapid antidepressant effects of NMDA antagonists. *Science* **329**, 959–964 (2010).
94. Tang, M. *et al.* Hippocampal proteomic changes of susceptibility and resilience to depression or anxiety in a rat model of chronic mild stress. *Transl. Psychiatry* **9**, 1–12 (2019).
95. D, R. *et al.* Hippocampal extracellular matrix alterations contribute to cognitive impairment associated with a chronic depressive-like state in rats. *Sci. Transl. Med.* **9**, (2017).
96. iTRAQ-based quantitative analysis of hippocampal postsynaptic density-associated proteins in a rat chronic mild stress model of depression - ScienceDirect. https://www.sciencedirect.com/science/article/pii/S0306452215003371?via%3Dihub.
97. McEwen, B. S. *et al.* Mechanisms of stress in the brain. *Nat. Neurosci.* **18**, 1353–1363 (2015).
98. Perić, I., Costina, V., Stanisavljević, A., Findeisen, P. & Filipović, D. Proteomic characterization of hippocampus of chronically socially isolated rats treated with fluoxetine: Depression-like behaviour and fluoxetine mechanism of action. *Neuropharmacology* **135**, 268–283 (2018).
99. Gottschalk, M. G. *et al.* Fluoxetine, not donepezil, reverses anhedonia, cognitive dysfunctions and hippocampal proteome changes during repeated social defeat exposure. *Eur. Neuropsychopharmacol. J. Eur. Coll. Neuropsychopharmacol.* **28**, 195–210 (2018).
100. McEwen, B. S., Nasca, C. & Gray, J. D. Stress Effects on Neuronal Structure: Hippocampus, Amygdala, and Prefrontal Cortex. *Neuropsychopharmacology* **41**, 3–23 (2016).
101. Popoli, M., Yan, Z., McEwen, B. S. & Sanacora, G. The stressed synapse: the impact of stress and glucocorticoids on glutamate transmission. *Nat. Rev. Neurosci.* **13**, 22–37 (2012).
102. Yang, Y., Ju, W., Zhang, H. & Sun, L. Effect of Ketamine on LTP and NMDAR EPSC in Hippocampus of the Chronic Social Defeat Stress Mice Model of Depression. *Front. Behav. Neurosci.* **12**, (2018).
103. Strekalova, T., Spanagel, R., Bartsch, D., Henn, F. A. & Gass, P. Stress-Induced Anhedonia in Mice is Associated with Deficits in Forced Swimming and Exploration. *Neuropsychopharmacology* **29**, 2007–2017 (2004).
104. Strekalova, T. & Steinbusch, H. W. M. Measuring behavior in mice with chronic stress depression paradigm. *Prog. Neuropsychopharmacol. Biol. Psychiatry* **34**, 348–361 (2010).
105. Parsons, S., Kruijt, A.-W. & Fox, E. A Cognitive Model of Psychological Resilience. *J. Exp. Psychopathol.* **7**, 296–310 (2016).
106. Miyagi, T. *et al.* Psychological resilience is correlated with dynamic changes in functional connectivity within the default mode network during a cognitive task. *Sci. Rep.* **10**, 17760 (2020).
107. Pfarr, J.-K. *et al.* Brain structural connectivity, anhedonia, and phenotypes of major depressive disorder: A structural equation model approach. *Hum. Brain Mapp.* **42**, 5063 (2021).

108. Ng, L. H. L. *et al.* Ketamine and selective activation of parvalbumin interneurons inhibit stress-induced dendritic spine elimination. *Transl. Psychiatry* **8**, 1–15 (2018).
109. Shao, L.-X. *et al.* Psilocybin induces rapid and persistent growth of dendritic spines in frontal cortex in vivo. *Neuron* **109**, 2535-2544.e4 (2021).
110. Kim, E. J., Pellman, B. & Kim, J. J. Stress effects on the hippocampus: a critical review. *Learn. Mem.* **22**, 411–416 (2015).
111. Yang, C. *et al.* Mechanistic Target of Rapamycin–Independent Antidepressant Effects of (R)-Ketamine in a Social Defeat Stress Model. *Biol. Psychiatry* **83**, 18–28 (2018).
112. Suo, L. *et al.* Predictable Chronic Mild Stress in Adolescence Increases Resilience in Adulthood. *Neuropsychopharmacology* **38**, 1387–1400 (2013).
113. Xu, D. *et al.* Hippocampal mTOR signaling is required for the antidepressant effects of paroxetine. *Neuropharmacology* **128**, 181–195 (2018).
114. Sarbassov, D. D. *et al.* Rictor, a novel binding partner of mTOR, defines a rapamycin-insensitive and raptor-independent pathway that regulates the cytoskeleton. *Curr. Biol. CB* **14**, 1296–1302 (2004).
115. McCabe, M. P. *et al.* Genetic inactivation of mTORC1 or mTORC2 in neurons reveals distinct functions in glutamatergic synaptic transmission. *eLife* **9**, e51440 (2020).
116. Angliker, N. & Rüegg, M. A. In vivo evidence for mTORC2-mediated actin cytoskeleton rearrangement in neurons. *BioArchitecture* **3**, 113–118 (2013).
117. Zhu, P. J., Chen, C.-J., Mays, J., Stoica, L. & Costa-Mattioli, M. mTORC2, but not mTORC1, is required for hippocampal mGluR-LTD and associated behaviors. *Nat. Neurosci.* **21**, 799–802 (2018).
118. Kim, S.-G. *et al.* Tanc2-mediated mTOR inhibition balances mTORC1/2 signaling in the developing mouse brain and human neurons. *Nat. Commun.* **12**, 2695 (2021).
119. Li, X. & Jope, R. S. Is glycogen synthase kinase-3 a central modulator in mood regulation? *Neuropsychopharmacol. Off. Publ. Am. Coll. Neuropsychopharmacol.* **35**, 2143–2154 (2010).
120. Kondratiuk, I. *et al.* GSK-3β and MMP-9 Cooperate in the Control of Dendritic Spine Morphology. *Mol. Neurobiol.* **54**, 200–211 (2017).
121. Duda, P., Hajka, D., Wójcicka, O., Rakus, D. & Gizak, A. GSK3β: A Master Player in Depressive Disorder Pathogenesis and Treatment Responsiveness. *Cells* **9**, 727 (2020).
122. Beurel, E., Grieco, S. F. & Jope, R. S. Glycogen synthase kinase-3 (GSK3): Regulation, actions, and diseases. *Pharmacol. Ther.* **148**, 114–131 (2015).
123. Koo, J., Wu, X., Mao, Z., Khuri, F. R. & Sun, S.-Y. Rictor Undergoes Glycogen Synthase Kinase 3 (GSK3)-dependent, FBXW7-mediated Ubiquitination and Proteasomal Degradation. *J. Biol. Chem.* **290**, 14120–14129 (2015).
124. Evangelisti, C., Chiarini, F., Paganelli, F., Marmiroli, S. & Martelli, A. M. Crosstalks of GSK3 signaling with the mTOR network and effects on targeted therapy of cancer. *Biochim. Biophys. Acta BBA - Mol. Cell Res.* **1867**, 118635 (2020).
125. Vidal, R. *et al.* Targeting β-Catenin in GLAST-Expressing Cells: Impact on Anxiety and Depression-Related Behavior and Hippocampal Proliferation. *Mol. Neurobiol.* **56**, 553–566 (2019).

126. Wu, B., Crampton, S. P. & Hughes, C. C. W. Wnt Signaling Induces Matrix Metalloproteinase Expression and Regulates T Cell Transmigration. *Immunity* **26**, 227–239 (2007).
127. Reel, B. *et al.* The Regulation of Matrix Metalloproteinase Expression and the Role of Discoidin Domain Receptor 1/2 Signalling in Zoledronate-treated PC3 Cells. *J. Cancer* **6**, 1020–1029 (2015).
128. Hayashi, T., Rumbaugh, G. & Huganir, R. L. Differential regulation of AMPA receptor subunit trafficking by palmitoylation of two distinct sites. *Neuron* **47**, 709–723 (2005).
129. Lin, D. *et al.* Regulation of AMPA receptor extrasynaptic insertion by 4.1N, phosphorylation and palmitoylation. *Nat. Neurosci.* **12**, 879–887 (2009).
130. Wei, J., Liu, W. & Yan, Z. Regulation of AMPA Receptor Trafficking and Function by Glycogen Synthase Kinase 3 *. *J. Biol. Chem.* **285**, 26369–26376 (2010).
131. Hausser, A. & Schlett, K. Coordination of AMPA receptor trafficking by Rab GTPases. *Small GTPases* **10**, 419–432 (2019).
132. Purkey, A. M. & Dell'Acqua, M. L. Phosphorylation-Dependent Regulation of Ca2+-Permeable AMPA Receptors During Hippocampal Synaptic Plasticity. *Front. Synaptic Neurosci.* **12**, (2020).
133. Lee, H.-K., Takamiya, K., He, K., Song, L. & Huganir, R. L. Specific Roles of AMPA Receptor Subunit GluR1 (GluA1) Phosphorylation Sites in Regulating Synaptic Plasticity in the CA1 Region of Hippocampus. *J. Neurophysiol.* **103**, 479–489 (2010).
134. Lu, W. *et al.* Phosphorylation of Tyrosine 1070 at the GluN2B Subunit Is Regulated by Synaptic Activity and Critical for Surface Expression of N-Methyl-d-aspartate (NMDA) Receptors *. *J. Biol. Chem.* **290**, 22945–22954 (2015).
135. Wójtowicz, T. & Mozrzymas, J. W. Matrix metalloprotease activity shapes the magnitude of EPSPs and spike plasticity within the hippocampal CA3 network. *Hippocampus* **26**, 414 (2016).
136. Ruxton, G. D. & Neuhäuser, M. Improving the reporting of P-values generated by randomization methods. *Methods Ecol. Evol.* **4**, 1033–1036 (2013).
137. Kaliszewska, A., Bijata, M., Kaczmarek, L. & Kossut, M. Experience-dependent plasticity of the barrel cortex in mice observed with 2-DG brain mapping and c-Fos: effects of MMP-9 KO. *Cereb. Cortex N. Y. N 1991* **22**, 2160–2170 (2012).
138. Bijata, M., Wlodarczyk, J. & Figiel, I. Dystroglycan controls dendritic morphogenesis of hippocampal neurons in vitro. *Front. Cell. Neurosci.* **9**, 199 (2015).
139. Bernadzki, K. M. *et al.* Arhgef5 Binds α-Dystrobrevin 1 and Regulates Neuromuscular Junction Integrity. *Front. Mol. Neurosci.* **13**, 104 (2020).
140. Degasperi, A. *et al.* Evaluating Strategies to Normalise Biological Replicates of Western Blot Data. *PLOS ONE* **9**, e87293 (2014).

MAIN FIGURES

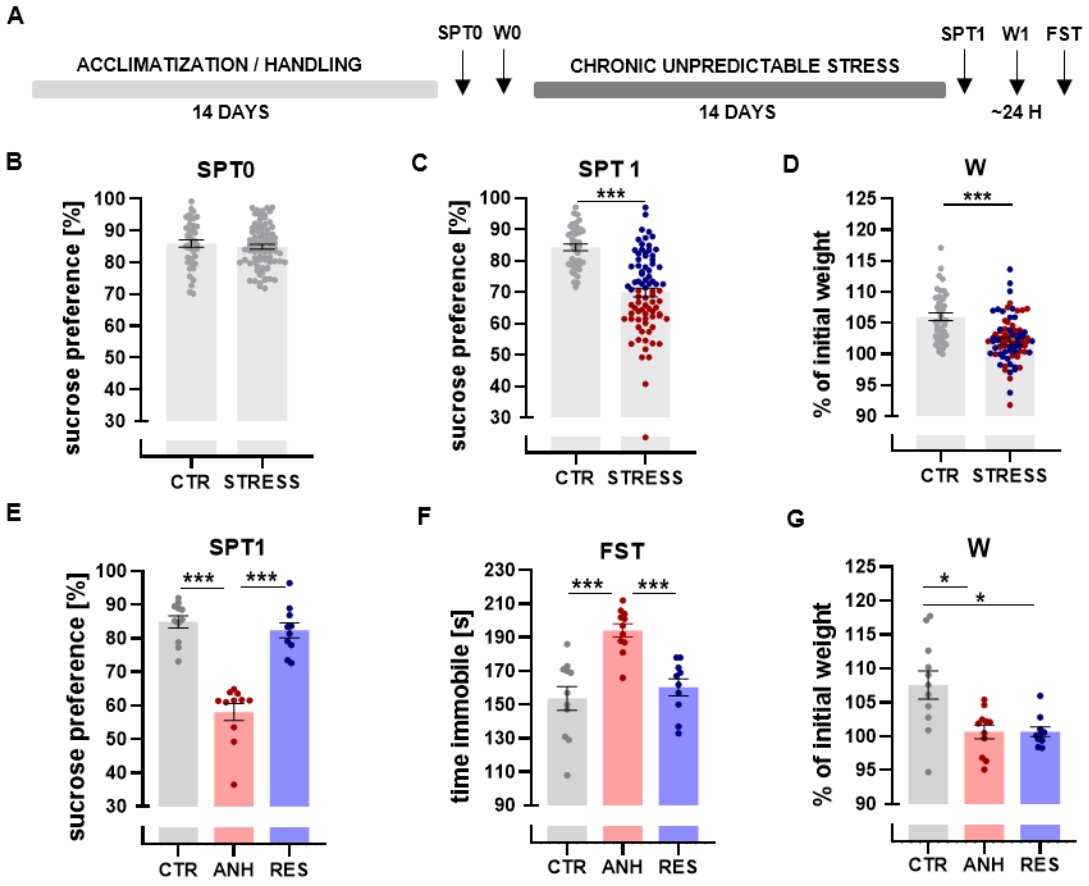

Figure 1. Behavioral evaluation of depressive-like behavior of anhedonic (ANH) and resilient (RES) animals following chronic unpredictable stress (CUS). (A) Schematic view of the experimental design of the CUS model. **(B)** Baseline sucrose preference test (SPT0). **(C)** Sucrose preference test after CUS (SPT1). **(D)** Body weight gain after CUS (W). **(E-G)** Behavioral parameters of representative animals chosen for the analysis of synaptic plasticity in the hippocampus. **(E)** Sucrose Preference Test after CUS (SPT1). **(F)** Forced swim test after CUS (FST). **(G)** Body weight gain after CUS (W). The data are presented as the mean ± SEM. *$p < 0.05$; ***$p < 0.001$.

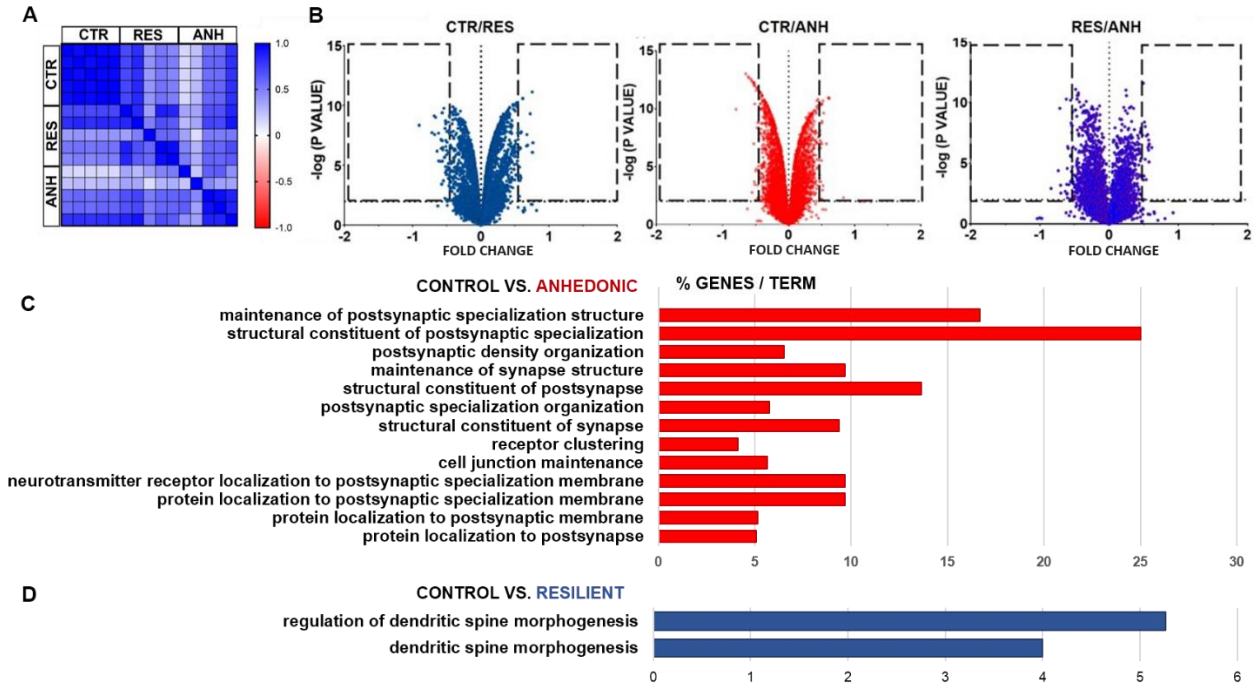

Figure 2. Analysis of differentially expressed synaptic proteins from proteomic profiling. (A) Matrix representation of Pearson correlation coefficients of protein abundances in 5 biological replicates. **(B)** Volcano plots represent changes in protein expression in CTR, ANH, and RES animals. The fold change log (base 2) is on the x-axis, and the negative false log discovery rate (p value) (base 10) is on the y-axis **(C-D)**. Kyoto Encyclopedia of Genes and Genomes (KEGG) bioinformatics analysis of the significantly altered signaling pathways of the ANH and RES groups. The p value negative log (base 10) is on the x-axis.

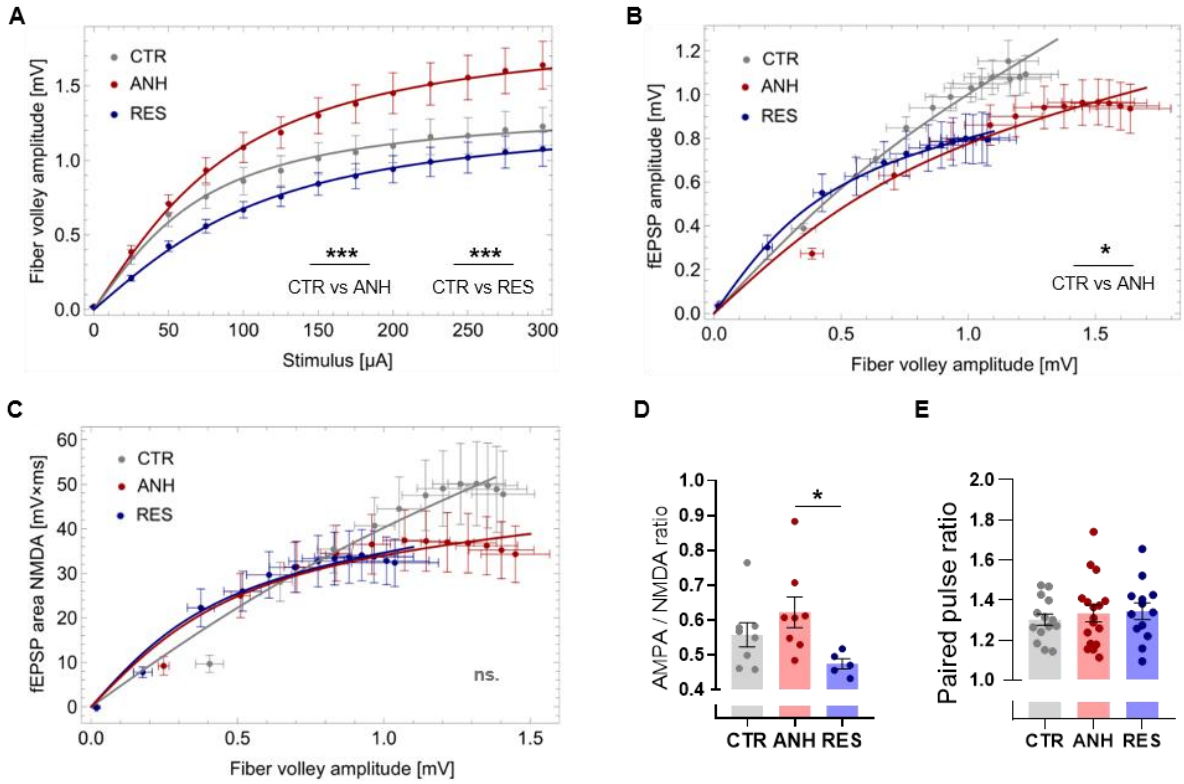

Figure 3. Chronic stress promotes differential changes in glutamatergic neurotransmission in the hippocampi of CTR, ANH, RES acute brain slices determined by **(A)** fiber volley amplitude, **(B)** fEPSP amplitude, **(C)** fEPSP NMDA area, **(D)** AMPA/NMDA ratio after DNQX application, **(E)** paired pulse ratio. **(A-C)** Statistics of the input–output relationships for fEPSPs evoked in response to monotonically increased current stimuli. **(A)** CUS resulted in significantly larger fiber volley amplitudes in the ANH group but significantly lower amplitudes in the RES than in the CTR group (one-way repeated measures ANOVA, with Dunnett's post-hoc test; experimental data were fitted with the function y(x) = a arctg$\frac{x}{b}$; see *Materials and Methods* for details). **(B-C)** fEPSP amplitudes and fEPSP area values normalized to fiber volley amplitudes. Experimental data were fitted with a mathematical function and compared for statistically significant differences by means of three-dimensional Monte Carlo simulations (see *Materials and Methods*, for details). **(B)** The magnitude of AMPAR-mediated fEPSPs recorded for the same fiber volley amplitude was significantly lower in the ANH but not the RES than in the CTR group. In contrast, **(C)** the NMDAR-mediated fEPSPs did not differ in the experimental groups. **(D)** The ANH group exhibited a higher AMPAR/NMDAR ratio estimated after DNQX application than that of the RES group (one-way ANOVA, see *Materials and Methods*, for details). **(E)** CUS did not affect the paired-pulse facilitation ratio. Data are presented as the mean ± SEM. *$p < 0.05$; ***$p < 0.001$.

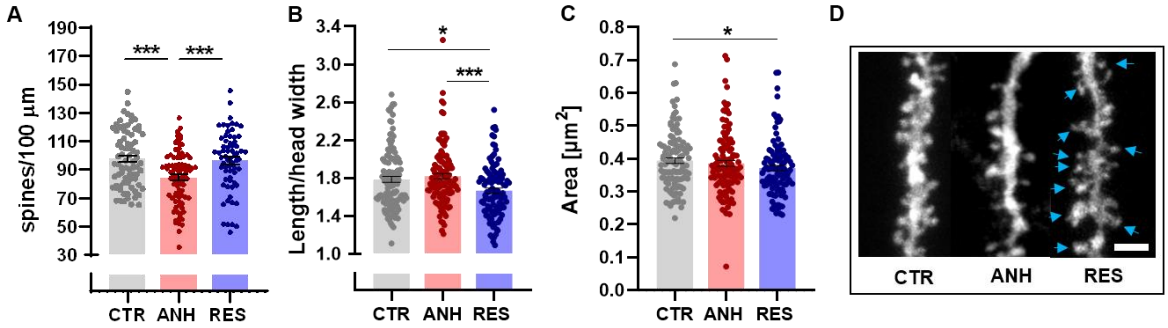

Figure 4. Chronic stress differentially affects the density and morphology of dendritic spines in the hippocampus of CTR, ANH, RES animals, including **(A)** spine density, **(B)** morphology in scale-free parameter (length/head width ratio) of relative morphometric changes, and **(C)** dendritic spine area: CTR N_{spines}=7735, $N_{dendrites}$=116, $N_{animals}$=5; ANH N_{spines}=7918, $N_{dendrites}$=120 $N_{animals}$=5; RES N_{spines}=7026 $N_{dendrites}$=107, $N_{animals}$=5 **(D)** representative confocal images of CTR, ANH, RES hippocampal CA1 dendritic segments. The arrows indicate the mushroom-shaped dendritic spines in the RES group. Scale bar=2 µm. Data are presented as the mean ± SEM. The points on the graphs represent the dendrite fragments in 1 field of view; *$p < 0.05$; ***$p < 0.001$ (nested analysis of variance with animals and spines).

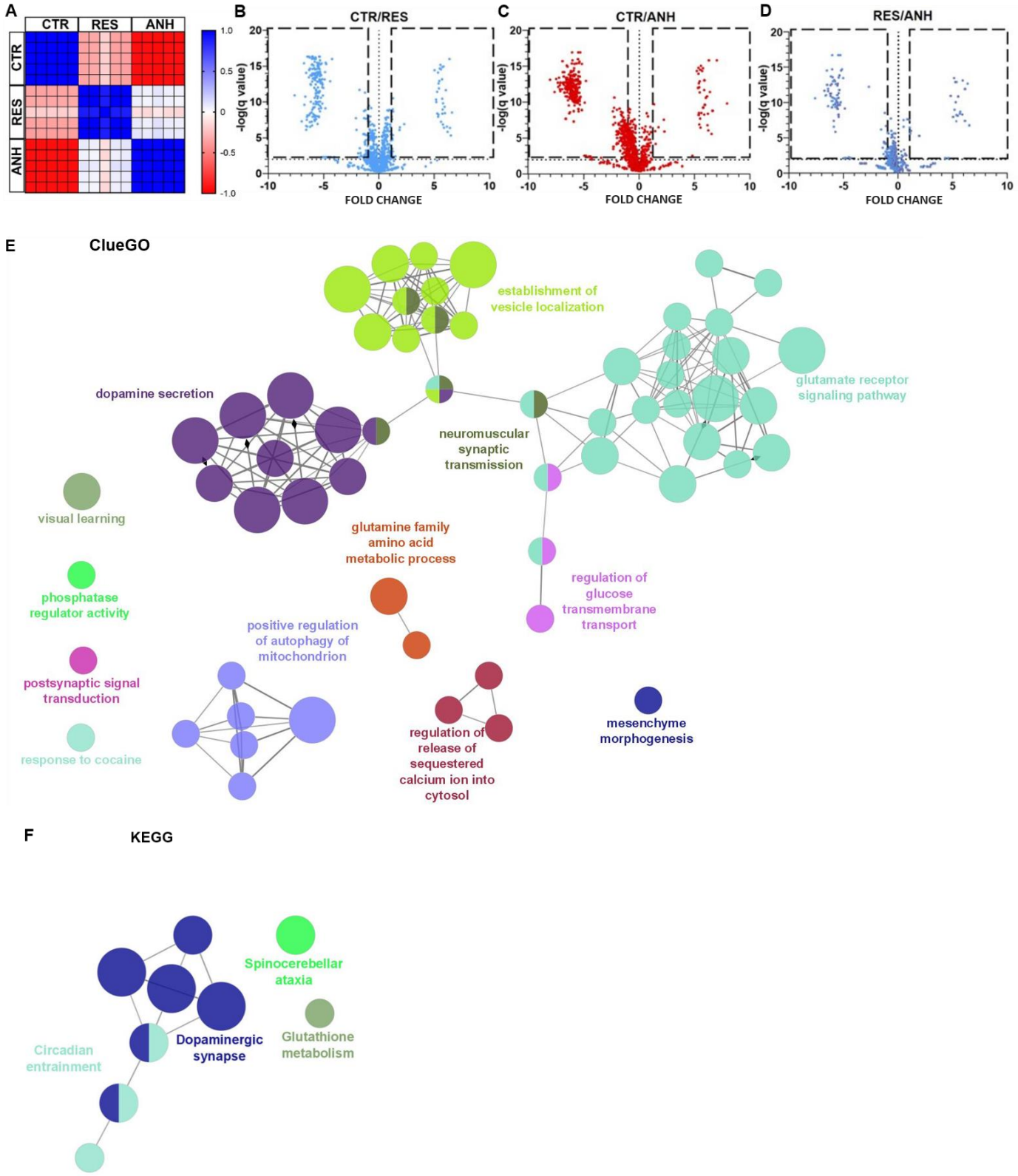

Figure 5. Analysis of differentially S-palmitoylated synaptic proteins from proteomic profiling. (A) Matrix representation of Pearson correlation coefficients of protein abundances in 5 biological replicates. **(B-D)** Volcano plots represent changes in protein S-palmitoylation in hippocampal synaptoneurosomes of

CTR, ANH, and RES animals. The fold change log (base 2) is on the x-axis, and the negative false log discovery rate (p value) (base 10) is on the y-axis. **(E)** Venn diagram comparisons of ClueoGO, and **(F)** KEGG bioinformatics analysis of S-PALM proteins characteristic of stress resilience. Functionally grouped networks are linked to their GO biological processes and KEGG pathways. Each circle (node) represents a biological term consisting of various related proteins/genes. The node size represents the enrichment significance. Terms that belong to the same pathway are marked with the same color, and terms associated with two different pathways are marked with two colors. The connectivity (edges) between the terms in the network is derived from the kappa score (indicates the similarity of associated genes shared by different terms). Thicker edges indicate stronger similarity. Diamonds represent directed edges that link parent terms to child terms. Only the name of the most significant term in each group is shown to reduce the overlay.

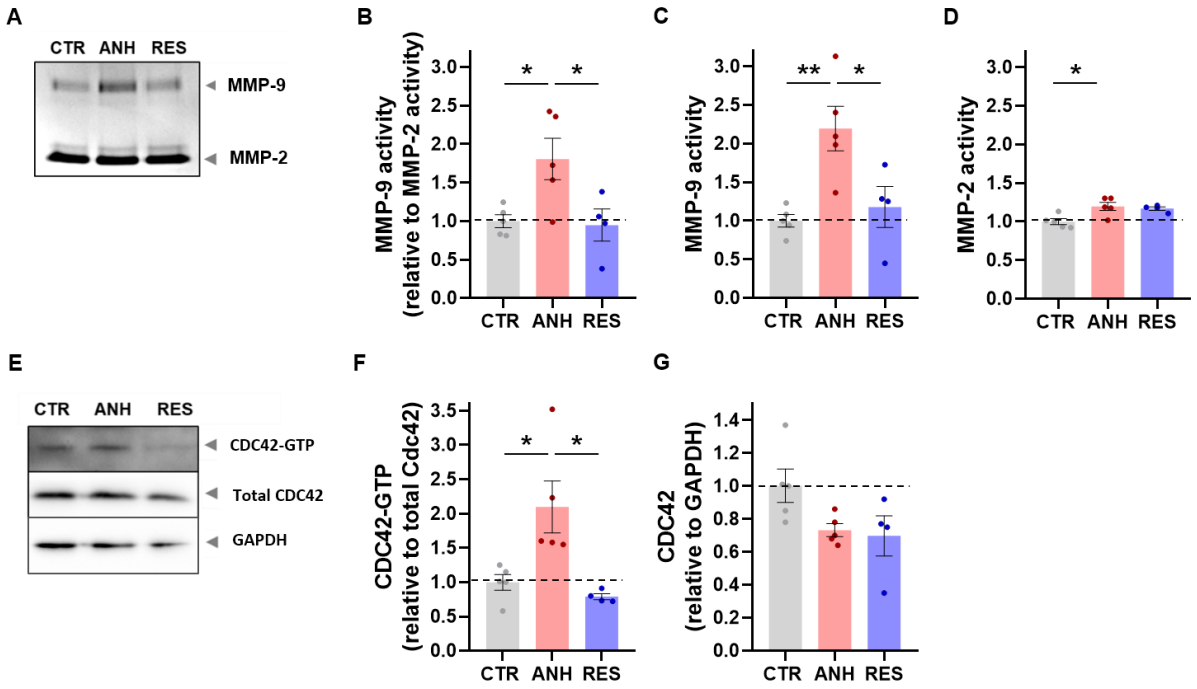

Figure 6. The MMP-9/CDC42 module is not activated in the hippocampus of stress-resilient animals. **(A)** Representative gelatinase activity in the hippocampi of control, anhedonic and resilient mice. **(B)** Quantification of the MMP-9/MMP-2 activity ratio, **(C)** MMP-9 activity, and **(D)** MMP-2 activity in the hippocampi of CTR, ANH and RES mice (N_{CTR}=5; N_{ANH}=5; N_{RES}=4). **(E)** Representative Western blot showing activated CDC42 (CDC42-GTP) and total CDC42 levels in the hippocampi of CTR, ANH and RES mice. **(F)** Quantifications of CDC42 activity as the ratio of CDC42-GTP to total CDC42 levels and **(G)** CDC42 levels normalized to GAPDH determined from the Western blot (N_{CTR}=4 N_{ANH}=4, N_{RES}=4). The data are presented as the mean ± SEM; *$p < 0.05$; **$p < 0.01$ (one-way ANOVA followed by Sidak's multiple comparisons test).